Roles of Re and Cs Promoters and Organochlorine Moderators in the Synthesis of Ethylene Oxide on Ag-based Catalysts

Andrew Hwang,[a] Jennifer Klaucke,[b] Carlos Lizandara-Pueyo,[c] Andrey Karpov,*[b] and Enrique Iglesia*[a, d]

C_2H_4–O_2 reactions form ethylene oxide (EO) on Ag nanoparticles dispersed on α-Al_2O_3 and promoted with alkali and other elements, with Re and Cs most frequently used in practice. Traces of alkyl chlorides (e.g., C_2H_5Cl) and alkanes in much larger amounts are added to reactants to balance the rate of deposition and removal (and the coverage) of Cl adatoms (Cl*) on Ag surfaces. Such Cl adlayers retain Ag surface ensembles that form O_2-derived intermediates that favor EO synthesis, but typically decrease O_2 activation rates. A series of Ag/α-Al_2O_3 catalysts (with and without Re or Cs) are used here to examine the role of promoters and Cl moderators through an analysis of the effects of reaction conditions and C_2H_5Cl levels using convection-reaction constructs and a mechanistic formalism that considers O_2 (as chemisorbed O_2*) as the reactant in EO synthesis through one electrophilic O-atom, with the second O-atom (O*) acting as a unselective nucleophile that must be scavenged by a sacrificial reductant (C_2H_4 or EO); such channels are precluded by any intervening O_2 dissociation events (that form two O*). O_2 consumption rates in C_2H_4–O_2 reactions decrease 10-fold upon exposing Ag/α-Al_2O_3 to C_2H_5Cl, evincing persistent Cl* species that block active sites and require $>10^4$ C_2H_4 oxidation turnovers to be removed. Activation barriers do not change but relative rates of epoxidation versus combustion increase in the presence of this refractory Cl* adlayer, which reduces the number and shrinks the size of available site ensembles without altering their intrinsic reac-

tivity for O_2 activation to form O_2* but attenuating rates of its subsequent dissociation. Refractory O* adlayers also form on Ag surfaces, as shown by the accumulation of persistent O* species upon exposing reduced Ag particles to N_2O. Inter-atom repulsive forces weaken O* binding and destabilize N_2O decomposition transition states to eventually allow stable N_2 and O_2 evolution for catalytic N_2O decomposition, which occurs at landing ensembles formed at interstices of refractory adlayers. Cl* forms denser adlayers than O*, as evidenced by a 10-fold decrease not only to C_2H_4–O_2 rates but also to N_2O stoichiometric and catalytic rates and O* uptakes. The occasional evolution of O_2, which forms larger landing ensembles that more readily form 2O* from O_2, occurs with higher frequency from O* than mixed O*/Cl* adlayers, and this effect of Cl* to inhibit (O–O)* dissociation is demonstrated in CO probe reaction studies, which show that highly reactive bound dioxygen species are retained to a greater extent when adlayers comprise both Cl* and O*. Re and Cs do not influence the nature of such adlayers but increase and decrease, respectively, the number of acid sites and selectivity losses via EO combustion. Their respective domains may also block a modest fraction of Ag surfaces without consequences on intrinsic O_2 activation rates or EO selectivities. The effects of Re beyond those reported here may emerge upon synthetic protocols that alter Re location and Ag–Re intimacy to enable channels which utilize both O-atoms in epoxidation.

1. Introduction

Ethylene oxide (EO) is an essential chemical intermediate in the production of pharmaceuticals, agrochemicals, and personal care chemicals through intermediate molecules such as (poly)ethylene glycols, alcohol ethoxylate and ethoxysulfate surfactants, and ethanolamines. EO has been an article of commerce since the deployment of the chlorohydrin process in

[a] Dr. A. Hwang, Prof. Dr. E. Iglesia
Department of Chemical and Biomolecular Engineering
University of California, Berkeley
Berkeley, California 94720 (USA)
E-mail: iglesia@berkeley.edu

[b] J. Klaucke, Dr. A. Karpov
Catalysis Research
BASF SE
Ludwigshafen, Rhineland-Palatinate 67059 (Germany)
E-mail: andrey.karpov@basf.com

[c] Dr. C. Lizandara-Pueyo
California Research Alliance
BASF Corporation
Berkeley, California 94720 (USA)

[d] Prof. Dr. E. Iglesia
Charles D. Davidson School of Chemical Engineering
Purdue University
West Lafayette, Indiana 47907 (USA)

ChemCatChem

Research Article
doi.org/10.1002/cctc.202301369

**Chemistry
Europe**
European Chemical
Societies Publishing

1914.[1] Current aerobic EO synthesis uses Ag-based solids as catalysts in a process first reported in 1931[2] and widely used today[3–5] as one of the largest scale catalytic oxidation reactions.[6] Ag-based catalysts are supported on very low surface area α-Al_2O_3,[3–5] in contrast with the bulk Ag catalysts used in catalytic oxidation of methanol (to formaldehyde) and ethylene glycol (to glyoxal).

Process and catalyst developments have significantly increased EO selectivities and led to greater energy and C-atom efficiencies and smaller carbon footprints. These advances have required the addition of several promoters and moderators. Alkyl chlorides are used ubiquitously to deliver Cl-containing species that act as moderators. The use of pure O_2 (instead of air) has enabled operations at higher C_2H_4 pressures and space velocities (by avoiding the continuous introduction of N_2), which allows lower single-pass C_2H_4 conversions and higher EO selectivities. Furthermore, this makes it possible to use CH_4 (instead of N_2) as unreactive diluent; its high thermal conductivity enables greater reactor productivities and broadens flammability envelopes, thus preventing thermal runaway.[3–5] These process improvements, together with increasingly complex and diverse promoter packages, have led to continuous improvements in EO selectivities (from about 70% in 1965 to about 90% in 2023[7]).

EO synthesis occurs via pathways (Scheme 1) involving reaction channels that form EO (Reaction I) or CO_2 and H_2O (II) from C_2H_4–O_2 reactants. Secondary EO reactions occur via either direct combustion (to CO_2 and H_2O; III) or EO isomerization or hydrolysis to form products (acetaldehyde or ethylene glycol, denoted as $\mathcal{I}$; IV)[8] that readily combust (V) at EO synthesis temperatures on Ag-based catalysts.[9–11] Acetaldehyde and ethylene glycol are present at trace (or undetectable) levels in effluent streams.[4,9,12] Such kinetic networks (Scheme 1) have guided the search for catalysts and conditions that disfavor C_2H_4 combustion (II) and secondary EO reactions (IV and V), with the latter often considered to occur at Brønsted or Lewis acid sites introduced by supports, promoters, or Cl-containing moderators.

The rate ratios that determine EO selectivities are influenced by promoter mixtures that can alter Ag surfaces and type and character of the bound O_2-derived species involved in electrophilic (epoxidation) and nucleophilic (H-abstraction) events. Such surface modifications influence r_I/r_{II} ratios, where r_j is the rate of Reaction j ($= I, II, ...,$ and V) in Scheme 1, which, in turn, determine primary selectivities. Some promoters, such as alkali
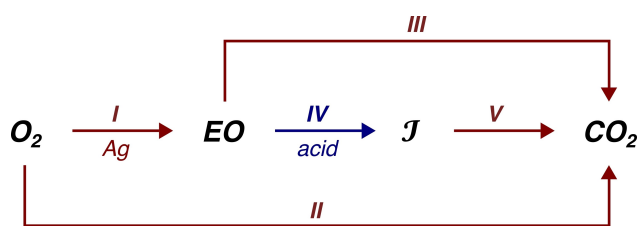
cations, titrate residual acid sites on α-Al_2O_3, thus decreasing r_{IV}/r_I and the extent to which EO selectivities decrease as O_2 and C_2H_4 conversions increase, whether such conversions are varied by changing temperature, residence time, or alkyl chloride concentrations. The consequences of several promoters for primary and secondary reactions were enumerated in a recent review,[13] but the variety of composition used in the most effective combinations of promoters is likely to cause unrecognized synergistic and antagonistic interactions among them. Such complexity prevents unequivocal insights into the location, role, and interactions of these components, as well as their mechanism of function, thus hindering the emergence of more precise (and plausibly simpler) design criteria. This is evident from the large number of inorganic promoters, each introduced at atomic ratios (*Ag/X*; *X* denotes the element used) of 10^2–10^4 in practical formulations.[14–16] The formidable history of success brought forth by empirical approaches, guided by statistical analysis, design of experiments, and high throughput experimentation,[17–19] is unlikely to continue unabated without more precise assessments of the synergies and incompatibilities among an increasing number of promoters. The most effective catalysts include several alkali cations (Li, K, Cs, ...), oxides of transition metals (Mn, Mo, W, Re, ...), and, in some cases, S-compounds as sulfates. Among these, Cs and Re appear ubiquitously among modern EO catalysts since the time of their respective discoveries as effective promoters.[20]

The effects of Cs on Ag powders[21–23] and Ag/α-Al_2O_3 samples[24–28] have been attributed to electronic effects[22,23,25] that inhibit EO isomerization on Ag[21] and titration of acid sites on α-Al_2O_3 supports.[24,27,28] The effects of Re[20] typically occur in synergistic combinations with Cs, which appears to titrate ReO_x-derived acid sites. Their combination led to EO selectivities exceeding 85.7% (C-basis),[29] a value thought unattainable based on analogies with monooxygenase (MO) enzymes; in such systems, each O_2 provides one electrophilic O-atom that adds to the C=C bond in C_2H_4 to form EO, but the other O-atom acts as a nucleophile and must be removed by a sacrificial reductant (C_2H_4 in EO synthesis and NADH in methane monooxygenase[30]). This corresponds to three EO molecules per one CO_2 molecule (and one H_2O molecule), a selectivity defined in Section 2.1 as the "monooxygenase limit".[29]

The presence of either or both Re and Cs promoters on electrolytic Ag powders (200,000 *Ag/Re* and 400,000 *Ag/Cs* atom ratios)[31] led to higher EO rates and selectivities, with values above the MO limit ($>$86% (C-basis) at 2% C_2H_4 conversion), compared to unpromoted powders. The copromoted sample gave the highest rate and selectivity, and this synergistic effect was attributed (based on work function data) to an optimal, but fortuitous, balance between electron transfer from Ag to Re oxyanions and from Cs oxyanions to Ag, leading to bound O adatoms (O*) with an electrophilic character conducive to epoxidation events. Similar directional effects were reported on Ag/α-Al_2O_3,[32] but their magnitudes differed depending on the deposition sequence of the Re and Cs promoters. In these studies,[31,32] C_2H_4–O_2 reactions were not conducted with alkyl chloride moderators, but the effects of Re and Cs were also observed for EO synthesis on Ag/α-Al_2O_3 in

Scheme 1. Reaction network for C_2H_4–O_2 reactions on Ag-based catalysts. The products of acid-catalyzed ethylene oxide (EO) isomerization and hydrolysis are denoted as $\mathcal{I}$.

ChemCatChem

Research Article
doi.org/10.1002/cctc.202301369

Chemistry Europe

European Chemical
Societies Publishing

the presence of C_2H_5Cl.[33] X-ray diffraction and electron microscopy showed that neither Cs nor Re caused changes in the morphology of Ag crystallites, and X-ray photoelectron spectra indicated that Re decreases the electron density of O*. These authors conjectured that Cs^+ cations on Ag surfaces facilitated EO desorption and inhibited its secondary reactions. DFT calculations, performed both in the absence[34,35] and presence of Cl adatoms[36,37] on Ag_{20} clusters[34,36] and extended Ag(111) surfaces,[35,36] support previously proposed notions that anionic Re-oxo and cationic Cs moieties, when in atomic contact with Ag domains, can tune the electrophilicity of O* to increase C_2H_4 epoxidation and lower C_2H_4, EO, and CH_3CHO combustion rates.

Here, C_2H_4–O_2 reactions on a series of Ag/α-Al_2O_3 catalysts with and without Re and Cs promoters were performed in the absence and presence of C_2H_5Cl moderators. The effects of reaction conditions, promoter identity, and C_2H_5Cl concentrations on rate and selectivity were deconvoluted using chemical reactor analysis protocols and presented from the mechanistic vantage of monooxygenase enzymes, in which only one O-atom within O_2 effects electrophilic C_2H_4 epoxidation while the other nucleophilic O-atom is scavenged in a cascade of oxidation events that lead to combustion products.[29] This perspective elicits interpretations of selectivity from an O_2-basis, instead of the more customary and practical definition of C-based selectivity, and considers losses in EO selectivity as occurring either via O–O bond dissociation within the bound dioxygen intermediates (O_2*), which forms two equivalents of the nucleophilic oxygen (2O*), or via parasitic reactions between O* and EO, either through a bound precursor (e.g., EO*) or directly from the gas-phase, in primary and secondary surface sojourns.

These experiments show that C_2H_5Cl deposits persistent Cl adatoms on Ag surfaces (Cl*) to form a refractory Cl* adlayer, which decreases the number of site ensembles available for kinetically-relevant O_2 activation but does not alter their intrinsic reactivity, as evidenced by a 10-fold decrease in rate and only a negligible change to the activation barrier. More labile bound Cl species form at interstices of the adlayer to reversibly titrate the landing ensembles that turn over for C_2H_4–O_2 reactions. Upon removing C_2H_5Cl from reactant streams, removal of the persistent Cl* species requires durations of C_2H_4–O_2 reactions that correspond to $>10^4$ O_2 conversion turnovers. The refractory Cl* adlayer decreases not only the number of available site ensembles but also their size, which prevents O_2* dissociation and leads to higher EO selectivity in primary sojourns.

Refractory O* adlayers also form, evidenced here through the deposition of strongly bound O adatoms upon exposing bare reduced Ag particles to N_2O, which convey interatomic repulsion between O* species to weaken their binding and eventually allow recombinative desorption to occur at rates matching those for O* deposition such that steady-state N_2O decomposition catalysis is achieved. The presence of Cl* decreases O* uptakes as well as stoichiometric and catalytic N_2O decomposition rates, showing that Cl adatoms are more persistent than O adatoms and that mixed Cl*/O* adlayers are denser than those comprising solely O*. The increased adlayer

density decreases the average size of interstitial landing ensembles to inhibit O_2* dissociation and bimolecular surface reactions between EO* and O*, and thereby increase the utilization of electrophilic O-atoms for C_2H_4 epoxidation. Persistent Cl* species increase O*–O* mean distances to decrease the frequency of occasional recombinative desorption of 2O* within refractory adlayers or of O adatoms at interstitial site ensembles. The increased retention of O_2* is demonstrated using CO probe reactions which show that highly reactive bound O_2-derived species, which are readily consumed by CO to form CO_2 at 233 K, are only formed on surfaces with refractory O*/Cl* adlayers and only retained with appreciable coverages when O_2 is present in the fluid-phase.

Re and Cs promoters when introduced to Ag/α-Al_2O_3 catalysts using the preparation and treatment protocols described herein, and at levels resembling those in commercial formulations (~300:1 atom ratios of bulk Ag to Re or Cs), do not alter the intrinsic reactivity of these site ensembles either for O_2 activation or for the selectivity-determining rate constant ratio that determines primary selectivity. They form domains that obstruct C_2H_4–O_2 reactants from accessing Ag surfaces and affect selectivity by altering rates of secondary EO consumption channels that lead to selectivity losses in subsequent sojourns. Re introduces additional acid centers that catalyze isomerization and hydrolysis of EO products into CH_3CHO and $(CH_2OH)_2$ species that are more readily combusted. Cs neutralizes acid centers, both on the support and introduced by Re, to attenuate selectivity losses in secondary EO sojourns. These results show that the speciation of promoter domains and/or their proximity to Ag surfaces, which are affected by the manner in which the promoters are introduced and the catalysts are treated prior to C_2H_4–O_2 reactions, affect their efficacy to utilize both O-atoms for electrophilic C_2H_4 epoxidation and thereby enhance EO selectivity to values exceeding the monooxygenase limit.

2. Results and Discussion

2.1. A mechanistic vantage point for EO formation from C_2H_4–O_2 reactants on Ag catalysts

The elementary steps and reaction channels involved in the aerobic oxidation of C_2H_4 to form EO and parasitic CO_2 and H_2O co-products can be viewed through the different O_2 usage efficiency of monooxygenase and dioxygenase enzymes.[29,38]

Dioxygenases use both O-atoms in O_2 in electrophilic insertion events[39–41] leading to the EO formation stoichiometry:

$$O_2 + 2C_2H_4 \rightarrow 2C_2H_4O \tag{1}$$

Known dioxygenases do not deliver, however, both O-atoms into two molecules of the same substrate, as in Equation 1, but either one O-atom each into two distinct substrates (one of them typically an α-keto acid; intermolecular) or both O-atoms into one substrate molecule (to form dihydroxylation products; intramolecular). In each case, the use of both O-atoms in

ChemCatChem

Research Article
doi.org/10.1002/cctc.202301369

**Chemistry
Europe**
European Chemical
Societies Publishing

oxidative C—C cleavage and (di)hydroxylation reactions requires the action of a conjugate base, either that for the α-keto acid or for an amino acid bound at or near the active center.

Monooxygenases use one O-atom in O_2 as an electrophilic reagent and rapidly scavenge the other (nucleophilic) O-atom with a sacrificial reductant (a H^+ together with NAD(P)H to form a very reactive proton-hydride source), to avoid its parasitic reactions with the substrate.[30,42–44] In Ag-catalyzed EO synthesis, this monooxygenase selectivity limit is achieved when one O-atom in O_2 is used for epoxidation (the electrophilic O-atom)[45,46] and the nucleophilic O-atom is consumed in a combustion cascade to form CO_2 and H_2O; the resulting "monooxygenase" overall stoichiometry is then:

$$O_2 + \frac{7}{6}C_2H_4 \rightarrow C_2H_4O + \frac{1}{3}CO_2 + \frac{1}{3}H_2O \qquad (2)$$
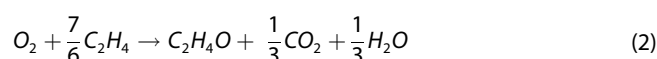
Scheme 2 depicts a three-step sequence for the monooxygenase perspective. O_2 binds onto a vacant site (*) to form a bound dioxygen intermediate (O_2*), in which electrophilic oxygen reacts with C_2H_4 to form EO and a bound O-atom (O*) as the nucleophilic oxygen. The scavenging of six O* species requires the sacrificial consumption of one C_2H_4 to complete a catalytic turnover. In contrast with monooxygenase enzymes, for which the substrate (e.g., CH_4 or squalene) and the sacrificial reductant ($H^+ +$ NAD(P)H) are different,[42] EO synthesis involves C_2H_4 as both the substrate and reductant.

This monooxygenase (MO) limit leads to a fractional C-based EO selectivity of 0.857. Measured selectivities divided by this MO limit (S_O) are then given in terms of molar yields of EO and CO_2 (Y_j, j = EO or CO_2) by:

$$S_O = \frac{(Y_{EO}/Y_{CO_2})}{3} \qquad (3)$$
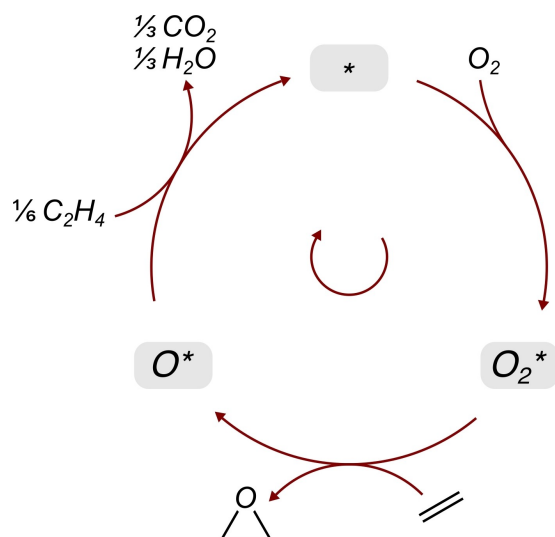
Scheme 2. A three-step sequence for monooxygenase-type primary C_2H_4–O_2 reactions (Eq. 2). O_2 activation on a bare site (*) forms a bound dioxygen intermediate (O_2*) that delivers an electrophilic O-atom into an alkene substrate via epoxidation, leaving behind a nucleophilic O adatom (O*) that is consumed in an oxidation cascade for C_2H_4 combustion.

S_O becomes unity when one O-atom in each O_2 is used exclusively in epoxidation and the other one consumed through sacrificial C_2H_4 combustion cascades. These S_O values complement the (more practical) C-based fractional selectivity (S_c) with one that is based on O-atoms; the two metrics are related by the following:

$$S_c = \frac{6 S_O}{6 S_O + 1} \qquad (4)$$

S_O values less than unity arise when primary EO products, instead of C_2H_4 substrates, are sacrificed in consuming O* and when O_2* dissociates to form 2O* instead of being consumed by C_2H_4 in epoxidation. S_O values greater than unity (supra monooxygenase selectivities) require the use of a nucleophilic oxygen in EO synthesis, presumably though its intervening conversion to an electrophilic form. An S_O value of about 1.5 corresponds to a C-based fractional selectivity (S_c value) of 0.90 (Eq. 4), which has been achieved in practice on Ag-based catalysts containing alkali (Li, Cs) and transition metal oxides (Mn, W, Re) using alkyl chlorides (1–10 ppm) as moderators;[14–19] these selectivities require that one out of every five nucleophilic O-atoms formed from O_2 in each EO synthesis turnover be used in another EO synthesis event, either directly or intervening conversion to an electrophilic form, reminiscent of the mediation by α-ketoglutaric acid or L-tyrosine in dioxygenases.[39] Examples of non-biological reaction systems that convert nucleophilic oxygen atoms into electrophilic ones include the use of (hypo)chlorite-based reagents and cocatalysts to modify the distribution of oxygen transfer agents (e.g., O^{2-}, OH^-, ClO^-, ClO_2^-)[47,48] and the role of NO_2(g) shuttles to convert oxygen adatoms on Pt surfaces to bound nitrate species that effect methane partial oxidation to dimethyl ether.[49]

In what follows, the reactions in Scheme 1 and the steps in Scheme 2 are used in plug-flow reactor formalisms to describe rates and selectivities in C_2H_4–O_2 reactions, to identify the rate constant ratios that determine selectivity, and to examine how such ratios are influenced by Re, Cs, and alkyl chlorides.

2.2. Reactor-level analysis of kinetic trends for C_2H_4–O_2 reactions on Ag-based catalysts

Previous kinetic studies of aerobic C_2H_4 oxidation on supported Ag catalysts in the absence[29,50,51] and presence of both organo-chlorine moderators (C_2H_5Cl) and inorganic promoters (Li, Na, Mn, Cs, Re)[12] showed that O_2 consumption rates could be described as nearly first-order in O_2 and zero-order in C_2H_4. Preliminary kinetic data for C_2H_4–O_2 reactions on the Re-promoted Ag/α-Al$_2$O$_3$ sample (18%wt. Ag, 380:1 Ag:Re; Sample **B** in Table 3) exhibit similar O_2 (strictly first-order) and C_2H_4 (nearly zero-order) dependencies (see Section S1 of the Supporting Information (SI)); these data were collected at conditions with O_2 as the limiting reactant (>5:1 C_2H_4:O_2), C_2H_5Cl moderators (4.0 Pa) present in reactant streams, minimal bed-scale gradients in reactant and product concentrations (achieved by operating at small fractional O_2 conversions

ChemCatChem

Research Article
doi.org/10.1002/cctc.202301369

Chemistry
Europe
European Chemical
Societies Publishing

(< 0.20) and by adding known amounts of CO_2 ($> 2:1$ $O_2:CO_2$) and H_2O ($> 20:1$ $O_2:H_2O$) at the reactor inlet), and negligible particle-scale concentration gradients (i.e., the rate measurements were not corrupted by interphase mass transport artifacts; see Section S2 (SI) for Mears' criterion calculations). These kinetic trends are consistent with O_2 activation at vacant Ag surface sites as the kinetically-relevant step (Scheme 2) and with O_2 consumption rates (r_{O_2}) given by:

$$r_{O_2} = (k_I + k_{II})\, P_{O_2} \equiv k_{1^\circ}\, P_{O_2} \tag{5}$$

where k_{1° is the sum of the apparent first-order rate constants for the monooxygenase-type reaction (k_I; Reaction I in Scheme 1; Eq. 2) and C_2H_4 combustion (k_{II}; Reaction II); here, r_{O_2} is normalized to the total amount of Ag within the catalyst such that k_{1°, k_I, and k_{II} all bear dimensions of "mol ((mol total Ag)·ks·kPa)$^{-1}$".

EO combustion rates on supported Ag catalysts[50,51] and Ag(111) single crystals[52] were found to be nearly first-order in EO and zero-order in O_2, and combustion of CH_3CHO, $(CH_2OH)_2$, and other oxygenates derived from EO (denoted by $\mathcal{I}$ in Scheme 1; Reaction V) were shown to proceed much more rapidly than that of EO (Reaction III) for Ag on alumina-[8,51] and silica-based[50,53] supports. These established kinetic and combustion reactivity trends show that EO consumption rates in secondary pathways (Reactions III and IV) are first-order in EO:

$$r_{2^\circ} = (r_{III} + r_{IV}) = \left(\frac{2}{5}k_{III} + \frac{\rho_{acid}}{\rho_{Ag}}\hat{k}_{IV}\right) P_{EO} \equiv k_{2^\circ}\, P_{EO} \tag{6}$$

where k_{2° is the apparent first-order rate constant (per total Ag) for the EO consumption reactions. The rate constant for the acid-mediated EO consumption channel ($\hat{k}_{IV}$; IV) is defined per acid site (denoted by the circumflex), and those for all the other reactions (k_I, k_{II}, and k_{III}), which are all mediated by Ag, are defined on a total-Ag basis. Thus, the ratio of molar densities of acid sites to total Ag atoms within the Ag-based catalyst (ρ_{acid} and ρ_{Ag}, respectively) appears in Equation 6. The resulting kinetic dependence of the rate ratio for primary and secondary pathways, $r_{O_2}/r_{2^\circ} \sim P_{O_2}/P_{EO}$, implies that secondary consumption of EO is limited by its activation on vacant surface sites.

The incorporation of these rate equations (Eqs. 5 and 6) into material balances for packed-bed reactors[54] leads to the following system of dimensionless ordinary differential equations:

$$\frac{dX}{d\lambda} = Da\,(1 - X) \qquad\qquad X(0) = 0 \tag{7}$$

$$\frac{dY_{EO}}{d\lambda} = Da\left[\frac{1}{1+\psi}\,(1 - X) - \omega\, Y_{EO}\right] \qquad Y_{EO}(0) = 0 \tag{8}$$

Here, X is fractional O_2 conversion and λ is a dimensionless axial position. The three dimensionless numbers parameterizing Equations 7 and 8 are the Damköhler number for primary reactions (Da), the ratio of rate constants at the primary

selectivity-determining branch point (ψ), and that for secondary versus primary reaction channels (ω):

$$Da = \frac{k_{1^\circ}\,\rho_{Ag}\,RT}{\tau^{-1}} \tag{9}$$

$$\psi = \frac{k_{II}}{k_I} \tag{10}$$

$$\omega = \frac{k_{2^\circ}}{k_{1^\circ}} = \frac{\left(\frac{2}{5}k_{III} + \frac{\rho_{acid}}{\rho_{Ag}}\hat{k}_{IV}\right)}{(k_I + k_{II})} \tag{11}$$

This definition of Da (Eq. 9) involves the gas constant (R) and a (volumetric) contact time ($\tau = V_{cat}/v$, where V_{cat} is the volume of catalyst within the packed-bed and v is the total gas flow rate) and is, as expected for first-order reactions, independent of reactant concentration. It represents a ratio between volumetric rates of O_2 activation and convective flux.

An asymptotic linear analysis of Y_{EO}/X (Section S3, SI) gives the following relationship for how the selectivity ratio (S_O, Eq. 3) varies with O_2 conversion (X):

$$S_O = \frac{1 - (\omega/2)\,X}{(1+2\psi) + (\omega/2)\,X} \tag{12}$$

Equation 12 predicts that S_O is independent of O_2 and C_2H_4 pressures and is only a function of X. The primary (single surface sojourn) selectivity ($S_O(X \to 0)$) depends solely on the ratio of apparent rate constants for the primary reactions (ψ, Eq. 10), and the local slope and curvature of S_O as a function of X depends on both ψ and the ratio of apparent rate constants for the secondary to primary reactions (ω, Eq. 11), because higher relative rates of EO synthesis in primary events result in higher EO concentrations, which, in turn, accelerate its consumption in subsequent sojourns.

This treatment (Eqs. 9–12) is used in the next two Sections to relate the observed effects of Cl, Re, and Cs on selectivity to the two relevant ratios of rate constants (ψ and ω). The mechanistic interpretations thereof, combined with the observed consequences of these moderators and promoters on O_2 consumption rates and the corresponding energy barriers, provide insight into how the identity and distribution of O_2-derived intermediates and the intrinsic reactivity patterns of sites involved in O_2 activation and secondary EO consumption pathways are altered by alkyl chloride moderators and inorganic promoters.

2.3. Irreversible effects of initial contact of Ag-based catalysts with alkyl chlorides on rates and selectivity

Figure 1a shows O_2 consumption rates (per mol of total Ag) at different temperatures in Arrhenius form (110 kPa O_2, 580 kPa C_2H_4, 16 kPa CO_2, 1.6 kPa H_2O, and 890 kPa CH_4) on Ag/α-Al_2O_3 (18%wt. Ag) without Cs or Re and without exposure to C_2H_5Cl before or during these measurements (Sample **A'**, Table 3;

ChemCatChem

Research Article
doi.org/10.1002/cctc.202301369

Chemistry Europe
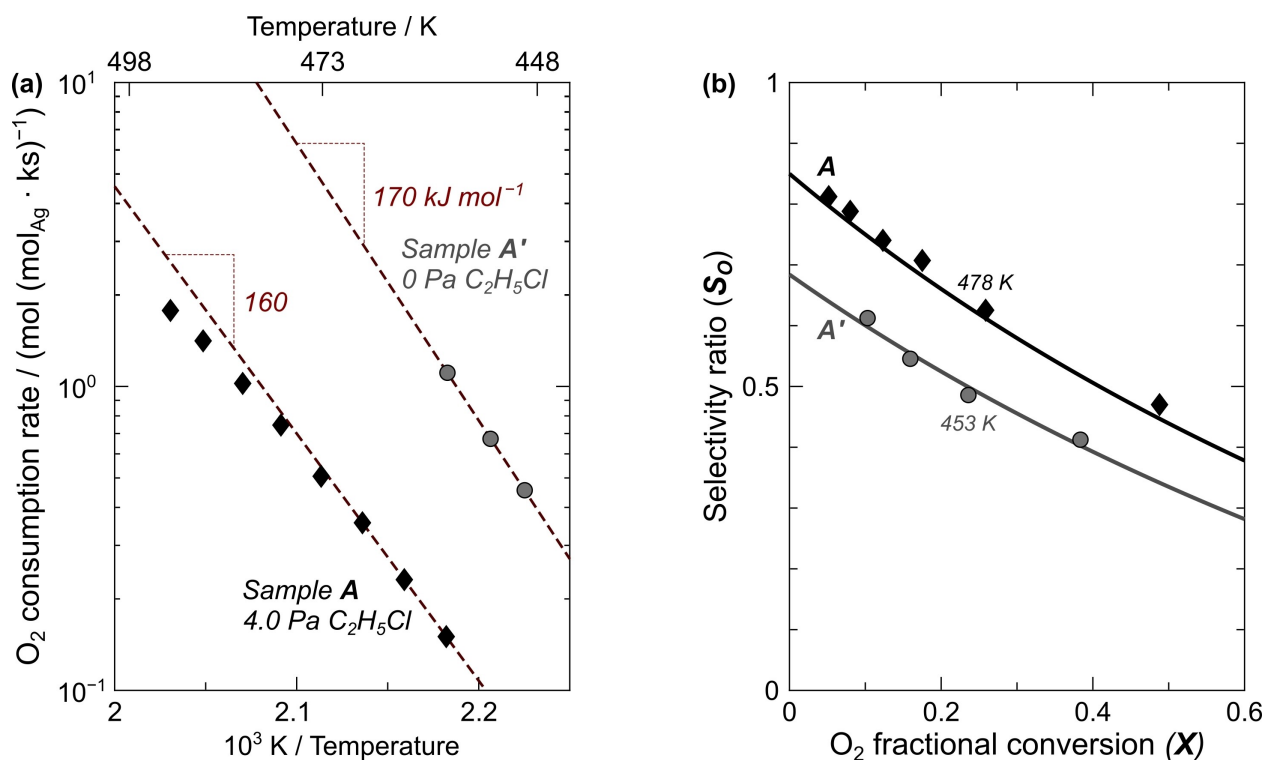European Chemical
Societies Publishing

Figure 1. (a) Arrhenius plot of O_2 consumption rates per total Ag in the catalyst samples and (b) selectivity ratios (S_O, Eq. 3) at different O_2 fractional conversions (X) for C_2H_4–O_2 reactions (433–493 K, 110 kPa O_2, 580 kPa C_2H_4, 16 kPa CO_2, 1.6 kPa H_2O, 890 kPa CH_4) on Ag/α-Al_2O_3 (18 % wt. Ag) performed in the absence (Sample **A'**, Table 3; circles) or presence of C_2H_5Cl (4.0 Pa; Sample **A**; diamonds) in reactant mixtures. The dashed lines in (a) represent those of best fit determined via linear regression on a semilogarithmic scale for $T < 470$ K, and the solid lines in (b) represent model predictions using best fit values of k_{II}/k_I and $k_{2°}/k_{1°}$ (Table 1) determined via non-linear regression of expanded $S_O(X)$ data set (Figure S2b) to Equation 12.

circles) and on the same samples exposed to C_2H_5Cl (4.0 Pa; Sample **A**; diamonds) during an initial "break-in" period (described in Section 4.2) and also during C_2H_4–O_2 reactions. Exposure to C_2H_5Cl decreased O_2 consumption rates nearly tenfold.

Surface-averaged particle diameters from SEM analysis ($\langle d_{SEM} \rangle$; Eq. 20; Section 4.1) for these two samples after reaction (see Section 4.2 for protocol used to extract samples from reactors) were slightly larger for Sample **A** (310 nm; Figure 2 (*bottom right*)) than Sample **A'** (240 nm, Figure 2 (*bottom left*)). The corresponding 1.3-fold decrease in the fraction of exposed Ag atoms (Đ = 0.0049 and 0.0038 for, respectively, **A'** and **A**; Eq. 21) cannot account for the observed 10-fold rate decrease upon C_2H_5Cl exposure. Archived rate data[55] for C_2H_4–O_2 reactions (513 K, 41 kPa O_2, 160 kPa C_2H_4, 5.3 kPa CO_2) on Ag/α-Al_2O_3 (35 % wt. Ag) conducted in the presence of C_2H_5Cl (1.9 Pa; and 2.1 kPa C_2H_6) show that O_2 consumption rates, when normalized to the number of exposed Ag atoms (estimated from SEM), decrease by less than a factor of 2 as $\langle d_{SEM} \rangle$ increases from 200 to 300 nm. These data imply that small changes in surface reactivity, as expected for such large particles, also cannot account for the 10× decrease in rate upon C_2H_5Cl admission (Figure 1a). The $\langle d_{SEM} \rangle$ value was smaller (140 nm, Figure 2 *(top)*) and the size distribution narrower in the as-prepared sample (which was treated in flowing N_2 at 563 K; Section 4.1) compared to the two "spent" samples, indicating that C_2H_4–O_2 reactions at the examined conditions, whether in

the presence (**A**) or absence (**A'**) of C_2H_5Cl, causes Ag crystallite growth. Sample **A** (310 nm) was collected after >450 h of C_2H_4–O_2 reactions at 458–493 K compared to <200 h at 433–458 K for **A'** (240 nm). These results are consistent with previous reports[55–57] which showed that the extent of particle growth increases with increasing duration and temperature in non-reducing environments. The formation of Cl adatoms (Cl*) on the Ag crystallites within Sample **A** may also contribute to its increased growth, as inferred from metal surface diffusion measurements on Au electrodes,[58,59] in which the presence of Cl* accelerates two-dimensional planar diffusion of surface Au atoms.

The effects of temperature and the apparent activation barriers are within experimental uncertainties on Samples **A'** ((170 ± 6) kJ mol^{-1}) and **A** ((160 ± 10) kJ mol^{-1}). Exposure to C_2H_5Cl during C_2H_4–O_2 reactions leads to significant coverages of Cl-derived species (e.g., Cl*[29,60]) and to much lower O_2 activation rates, but without detectable effects on the temperature dependence of kinetic and thermodynamic parameters for the elementary steps that determine such rates. Thus, the intrinsic reactivity of uncovered Ag ensembles for O_2 activation do not appear to be detectably influenced in their electronic character by interactions with bound Cl species.

The effects of C_2H_5Cl (Sample **A**) on O_2 consumption rates are initially unchanged by its removal, but gradually increase with time (Figure 3). The lack of a discontinuity in rate upon abrupt removal of the alkyl chloride moderator suggests that it
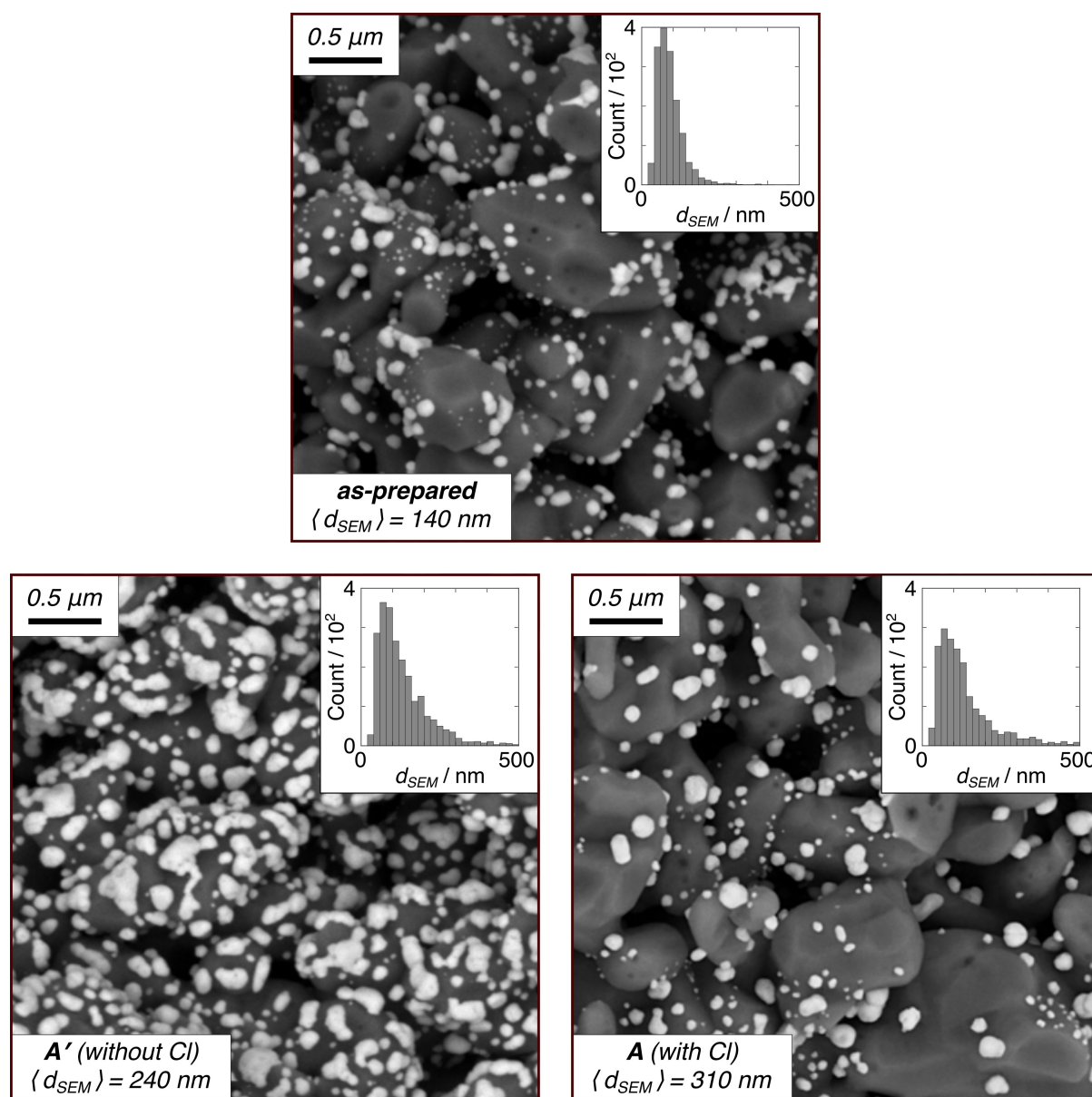
Figure 2. Representative scanning electron micrographs and particle size distributions for the as-prepared 18 % wt. Ag/α-Al$_2$O$_3$ sample (*top*) and those collected after C$_2$H$_4$–O$_2$ reactions in the absence (*bottom left*) and presence (*bottom right*) of C$_2$H$_5$Cl; see Section 4.2 for catalytic testing and sample retrieval protocols. More than 1500 particles were counted in the scanning electron micrographs (SEM) to calculate surface-averaged particle diameters ($\langle d_{SEM} \rangle$, Eq. 20).

and gaseous species derived therefrom are not involved in O$_2$ activation steps at these conditions. O$_2$ rates reach values that are 0.23 of those on Sample **A**′ after about 7 h, a period that corresponds to about ~5,000 O$_2$ activation turnovers (defined from rates on a per surface Ag atom basis, which were estimated using the measured fractional dispersion; Đ = 0.0038 for Sample **A**; Eq. 21). The linear extrapolation of this transient in rate to the rates on Sample **A**′ indicate that a period of about 50 h is required for removing the effects of exposure to C$_2$H$_5$Cl at these conditions. These data show that removal of Cl-derived species from Ag surfaces at these conditions requires time scales much longer than those for O$_2$ activation turnovers, as shown previously from concurrent measurements of rates of C$_2$H$_4$–O$_2$ reactions and of stoichiometric Cl removal on a commercial Ag/α-Al$_2$O$_3$ sample (35 % wt. Ag, with Li, Na, Mn, Cs, and Re promoters).[61] The significant titration of Ag surfaces by species derived from C$_2$H$_5$Cl (even at 4 Pa) cannot be reversed in the time scale of oxidation turnovers, but it appears to be ultimately reversed at much longer times through slow reactions of CH$_4$ and C$_2$H$_4$ with Cl*. For alkanes, these Cl-removal reactions are limited by homolytic C–H activation steps, as inferred from a correlation between C–H bond dissociation energies (of CH$_4$, C$_2$H$_6$, C$_3$H$_8$, and *i*-C$_4$H$_{10}$) and measured values of Cl* coverages that prevail during steady-state C$_2$H$_4$–O$_2$ reactions conducted in the presence of C$_2$H$_5$Cl and different scavengers.[62] Thus, in typical turnover times for aerobic C$_2$H$_4$ oxidation reactions on Ag surfaces, strongly bound Cl adatoms "irreversibly" titrate Ag surface sites, thus acting to
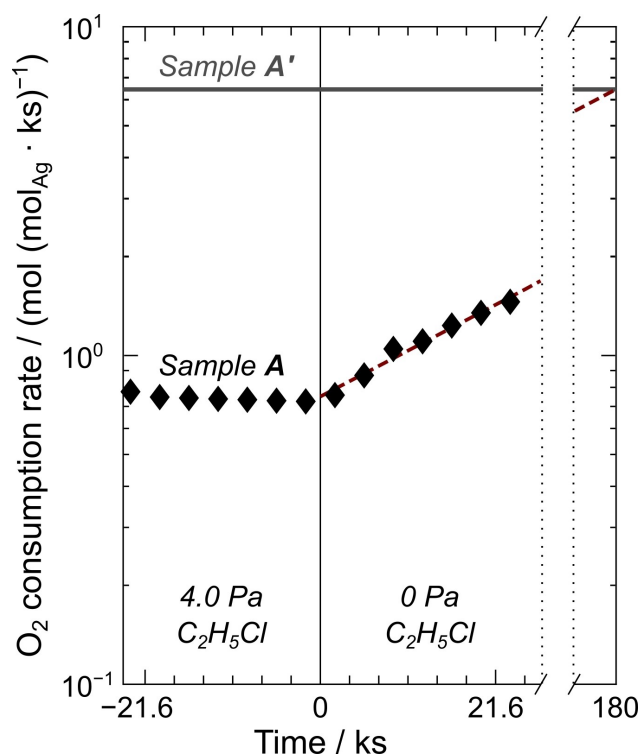
Figure 3. Temporal evolution of O_2 consumption rates before ($t < 0$) and after ($t > 0$) removing C_2H_5Cl from the inlet reactant stream ($t = 0$) during C_2H_4–O_2 reactions on Ag/α-Al_2O_3 (18%wt. Ag; Sample **A**, Table 3; 478 K, 110 kPa O_2, 580 kPa C_2H_4, 16 kPa CO_2, 1.6 kPa H_2O, 890 kPa CH_4). The dashed lines represent a linear regression of the rate data after removing C_2H_5Cl. The solid horizontal line denotes rates at the same conditions on the same Ag/α-Al_2O_3 sample but without exposure to C_2H_5Cl (Sample **A′**), which was estimated by extrapolating the Arrhenius dependence shown in Figure 1a (circles, ≤ 458 K), since this reaction temperature (478 K), in the absence of C_2H_5Cl, leads to reactor thermal instabilities that corrupt measured rates.

decrease the number of ensembles available for O_2 activation (as shown by the persistent ten-fold decrease in rates).

Figure 1b shows selectivity ratios (S_O, Eq. 3) at different (fractional) O_2 conversions (X) during C_2H_4–O_2 reactions on 18%wt. Ag/α-Al_2O_3; here, X was varied by changing reaction temperature: between 433–458 K and 458–493 K for Samples **A′** (circles) and **A** (diamonds; Table 3), respectively. Regardless of whether the sample was exposed to C_2H_5Cl, the asymptotic value of S_O at zero conversion is smaller than unity, thus precluding monooxygenase-like selectivities, in which one O-atom in O_2 forms EO (Step I in Scheme 3), while the other is scavenged by C_2H_4 to ultimately form combustion products (Eq. 2). These asymptotic S_O values of 0.68 and 0.85 for Samples **A′** and **A**, respectively, correspond to C-based fractional selectivities of 0.80 and 0.84 (Eq. 4). Selectivity losses in single surface sojourns can be ascribed to undesired events that occur after the kinetically-relevant O_2 activation step. If the initial epoxidation event results in a bound precursor to EO (EO*), then C_2H_4 combustion can occur when EO* reacts with O* (Step II(a)) before it desorbs (Step I(b)). It can also occur upon (O–O)* cleavage (Step II(b)), since the resulting two nucleophilic O adatoms (2O*) are removed via oxidation cascades to CO_2 and H_2O.

Secondary EO reactions account for the lower S_O as X increases, as depicted in Scheme 1. These trends effected through changes in temperature are similar when X was varied by changing extent of catalyst deactivation and C_2H_5Cl pressure; Figures 4 and 7b (Section 2.4) are analogous to Figure 1b, but show additional data with symbol shapes that correspond to the different manners in which X was varied. The kinetic and mechanistic implications of these coincidences are detailed in the subsequent Section within the context of the plug-flow reactor model developed in the previous Section, the reaction network in Scheme 1, and the elementary steps involving O_2* and O* depicted in Schemes 2 and 3.

The S_O versus X trends for Samples **A′** and **A** (as well as **B**, **C**, and **D**) can be regressed to the functional form of Equation 12 to obtain the k_{II}/k_I and $k_{2°}/k_{1°}$ parameters (Table 1). The ratio of rate parameters for C_2H_4 combustion (k_{II}; Reaction II, Scheme 1) and the MO-type epoxidation (k_I; Reaction I) is significantly smaller for Sample **A** (0.088) than Sample **A′** (0.23). The presence of Cl* attenuates loss of electrophilic O-atoms via C_2H_4 combustion by promoting the relative rate of EO* desorption (Step I(b) in Scheme 3) versus its parasitic reaction with
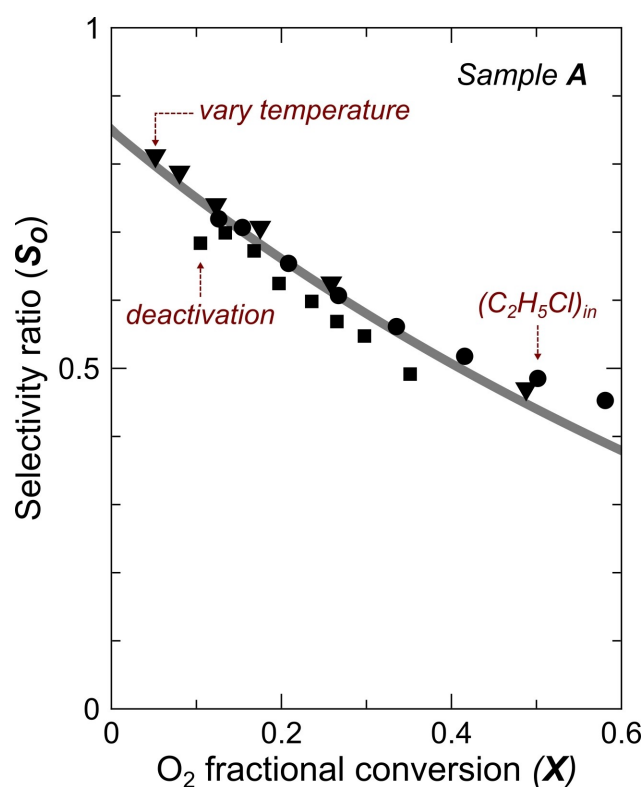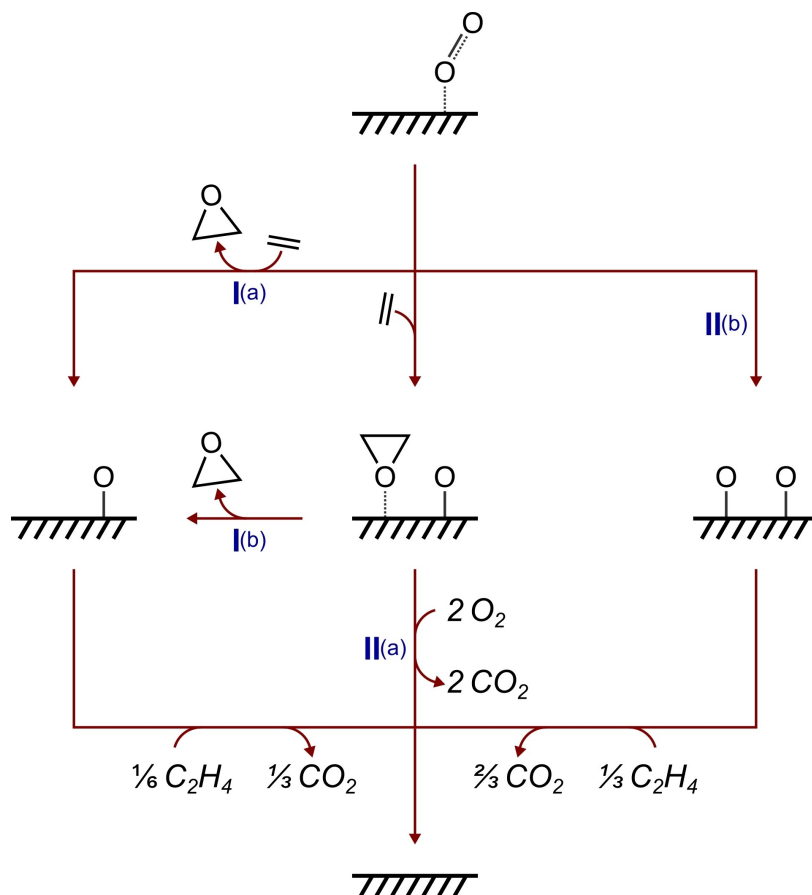

Figure 4. Selectivity ratios (S_O; Eq. 3) at different (fractional) O_2 conversions (X) for C_2H_4–O_2 reactions on Ag/α-Al_2O_3 exposed to C_2H_5Cl (18%wt. Ag; Sample **A**, Table 3). The triangles, squares, and circles denote data for which conversion was varied by changing (respectively) temperature (458–488 K; 110 kPa O_2, 4.0 Pa C_2H_5Cl), extent of deactivation (holding for 20 h after "break-in" protocols (Section 4.2); 473 K, 64 kPa O_2, 4.0 Pa C_2H_5Cl), and inlet C_2H_5Cl pressure (0.80–6.3 Pa; 478 K, 110 kPa O_2). All reactions were performed with excess C_2H_4 (340–580 kPa), with CO_2 (16 kPa) and H_2O (1.6 kPa) added to inlet streams, and at 1600 kPa with CH_4 as the balance gas. The solid trace represents the predictions from the model developed in Section 2.2 using k_{II}/k_I and $k_{2°}/k_{1°}$ values (shown in Table 1) obtained by regressing all selectivity data to the functional form of Equation 12.

ChemCatChem

Research Article
doi.org/10.1002/cctc.202301369

**Chemistry
Europe**
European Chemical
Societies Publishing

Scheme 3. Steps involved in single C_2H_4–O_2 surface sojourns on Ag-based catalysts for ethylene oxide (EO) synthesis. EO can form directly by reaction with the electrophilic O-atom in bound dioxygen species (O_2^*; Step I(a)) or through bound intermediates (EO*, I(b)). C_2H_4 combustion arises either when this precursor, instead of desorbing, reacts with nucleophilic O adatoms (O*; II(a)) or when O_2^* undergoes O–O cleavage (II(b)) before it can engage in C_2H_4 epoxidation. The H_2O co-products of combustion (1:1 CO_2:H_2O) are omitted for clarity.

Table 1. O_2 consumption rates (per total Ag; r_{O_2}) at 453 K and 478 K (110 kPa O_2, 580 kPa C_2H_4, 16 kPa CO_2, 1.6 kPa H_2O, 890 kPa CH_4; 0 and 4 Pa C_2H_5Cl for, respectively, Samples **A′** and **A–D**). Best fit values of rate constant ratios (k_{II}/k_I and $k_{2°}/k_{1°}$) determined via regression of selectivity (S_O, Eq. 3) versus conversion (X) trends (Figure 7b) to the functional form of Equation 12. The reported errors for k_{II}/k_I and $k_{2°}/k_{1°}$ are 95 % confidence intervals.

Sample	r_{O_2}/(mol (mol$_{Ag}$·ks)$^{-1}$)		k_{II}/k_I	$k_{2°}/k_{1°}$
	453 K	478 K	/–	/–
A′	0.70	6.3[i]	0.23 ($\pm$0.044)	1.5 ($\pm$0.40)
A	0.15	0.74	0.088 ($\pm$0.017)	1.3 ($\pm$0.12)
B	0.15	0.59	0.098 ($\pm$0.009)	1.6 ($\pm$0.081)
C	0.13	0.45	0.077 ($\pm$0.005)	1.0 ($\pm$0.048)
D	0.16	0.60	0.087 ($\pm$0.007)	0.89 ($\pm$0.045)

[i] Estimated using the Arrhenius dependence shown in Figure 1a (circles); this value is identical to that denoted by the solid horizontal line in Figure 3.

nucleophilic O adatoms (O*; Step II(a)) and/or inhibiting (O–O)* bond cleavage events that lead to 2O* (Step II(b)). Strongly bound Cl adatoms deplete not only the number of available surface site ensembles for O_2 activation (which lead to the ten-fold rate decrease, Figure 1a) but also, and more significantly, those for the bimolecular surface reactions (II(a) and II(b)) that lead to selectivity losses in single sojourns. Such "geometric effects" have been proposed previously[29] and supported by single-crystal studies,[60] which showed that pre-adsorbed Cl

adatoms decreased dissociative adsorption rates of O_2 on Ag(110) and increased desorption rates of bound precursors to EO on Ag(111).

The similar $k_{2°}/k_{1°}$ ratios for **A′** and **A** indicate that Cl species do not affect the relative rates of O_2-derived species with C_2H_4 (to form EO and CO_2) in primary reactions (Reactions I (Eq. 2) and II in Scheme 1) and with EO (to ultimately form combustion products) in secondary reactions (Reactions III, IV, and V). Taken together with the effects of Cl adatoms on primary selectivities

ChemCatChem

Research Article
doi.org/10.1002/cctc.202301369

**Chemistry
Europe**
European Chemical
Societies Publishing

(k_{II}/k_I), these results indicate that the steps that determine selectivity in secondary surface sojourns involve the same O_2-derived intermediates, which bear electrophilic and/or nucleophilic O-atoms, as those in primary sojourns (O_2* and O* in Schemes 2 and 3).

In the next section, the effects of C_2H_5Cl pressure and the number of available Ag surface sites on selectivity are compared with those of temperature to show their universality. The same reaction network (Scheme 1), reactor model (Section 2.2), and elementary steps (Schemes 2 and 3) used and developed here to describe the effects of strongly bound Cl adatoms on O_2 rates and primary and secondary selectivities are extended to the Re- and Cs-containing samples to elucidate functions of these inorganic promoters in EO synthesis processes.

2.4. Consequences of C_2H_5Cl pressure and of Re and Cs promoters for O_2 activation rates and primary and secondary selectivities

Figure 4 shows S_O values (Eq. 3) at different O_2 conversion levels (X) for C_2H_4–O_2 reactions (458–488 K, 60–110 kPa O_2, 340–580 kPa C_2H_4, 16 kPa CO_2, 1.6 kPa H_2O, 890–1200 kPa CH_4) with 0.80–6.3 Pa C_2H_5Cl added to the inlet stream on Ag/α-Al_2O_3 (Sample A, Table 3; 453–493 K and 4.0 Pa C_2H_5Cl during "break-in", Section 4.2). O_2 conversions were varied through changes in temperature (triangles), extent of catalyst deactivation during the first reaction period after "break-in" protocols (squares), or C_2H_5Cl concentrations (circles). O_2 consumption rates decreased with increasing C_2H_5Cl levels in the inlet stream (Figure 5). The O_2 inlet molar rates were kept the same in all these experiments (2.9 (mol O_2)·((mol total Ag)·ks)$^{-1}$), and so, O_2 conversion levels (X) decreased concomitantly with increasing C_2H_5Cl concentration. Selectivity trends with changes in C_2H_5Cl concentrations were the same as with changes in conversion caused by temperature changes or initial deactivation.

The two parameters (k_{II}/k_I and $k_{2°}/k_{1°}$) and the functional form of Equation 12 accurately describe effects of X on S_O, irrespective of how X was varied. These similar trends indicate that rates are indeed proportional to O_2 and largely insensitive to C_2H_4 for primary C_2H_4 conversion reactions and only proportional to EO for secondary reactions (Eqs. 5–6). This suggests, in turn, that bound species derived from O_2 and EO are not present on Ag surfaces or acid centers at kinetically-detectable coverages during C_2H_4–O_2 reactions at these conditions. These circumstances would otherwise lead to a rate equation for primary reactions (r_{O_2}, Eq. 5) that is sub-linear in O_2 and sensitive to EO pressure and to one for secondary reactions ($r_{2°}$, Eq. 6) that is not strictly zero-order in O_2 or first-order in EO. These common $S_O(X)$ trends include changes in X imposed by different temperatures (triangles, Figure 4), thus requiring that the temperature effects on k_{II}/k_I and $k_{2°}/k_{1°}$ ratios be weak and that differences in activation barriers for numerator and denominator terms in each ratio be much smaller than the O_2 activation barrier (160 kJ mol^{-1}, Figure 1a). The number of Ag surface site ensembles available for O_2 activation decreases with
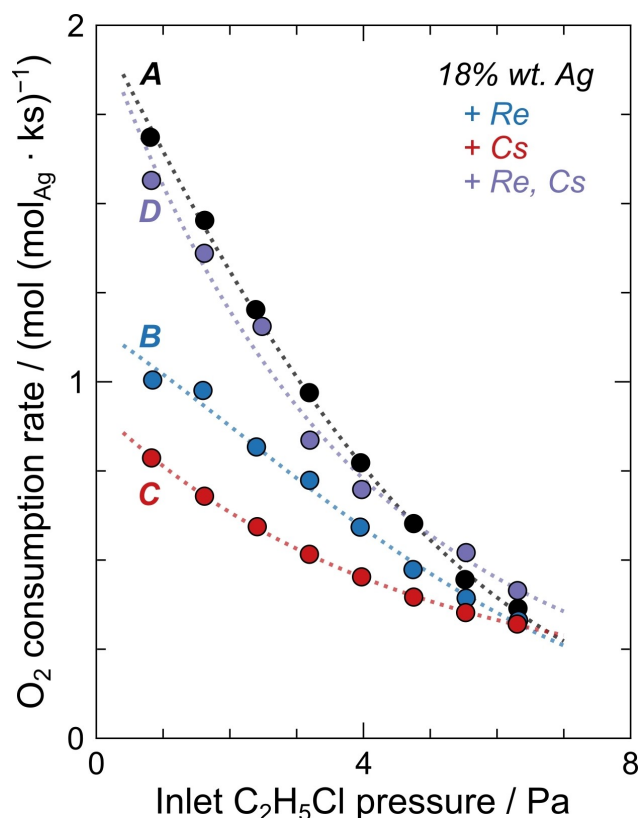

Figure 5. O_2 consumption rates, per total amount of Ag, versus inlet C_2H_5Cl pressure for C_2H_4–O_2 reactions (478 K, 110 kPa O_2, 580 kPa C_2H_4, 16 kPa CO_2, 1.6 kPa H_2O, 890 kPa CH_4) on 18 % wt. Ag/α-Al_2O_3 samples exposed to C_2H_5Cl with neither Re nor Cs promoters (Sample A, Table 3), with 380:1 Ag:Re (atom ratio; **B**), with 380:1 Ag:Cs (**C**), and with both Re and Cs (380:1 each; **D**). The dotted curves represent trend curves as visual guides.

increasing extent of deactivation and the coincidence in the $S_O(X)$ trends for deactivation (squares, Figure 4) and C_2H_5Cl pressure (circles) implies that the latter reflects a decrease in the number of "landing ensembles".

The kinetic effects of C_2H_5Cl levels (Figures 4 and 5) involve transient periods to reach steady-state (< 8 h; ~5,000 O_2 conversion turnovers) that are much shorter than for restoring Cl-free rates after C_2H_5Cl removal from inlet streams (Figure 3; ~50 h; ~40,000 turnovers); these transients appear to involve the removal and formation of Cl species that are more labile than the strongly bound Cl adatoms that prevent Ag surfaces from restoring their Cl-free state in Sample A'. Figure 6 is analogous to Figure 3 but depicts the shorter transients observed upon a two-fold increase in C_2H_5Cl concentrations (0.80 to 1.6 Pa). These "reversible" kinetic effects of Cl are likely to reflect the binding of Cl atoms at interstices within a refractory Cl adlayer, reminiscent of the weak binding of Cl at spaces intervening strongly bound Cl adatoms that form ordered structures on Ag(111) crystals,[63] thus allowing the covering and uncovering of Ag patches in response to changes in the levels of C_2H_5Cl in the contacting fluid phase. Such reversible binding serves to change the number of free "landing ensembles" within refractory Cl adlayers, but not their intrinsic reactivity for primary and secondary reactions (k_{II}/k_I and
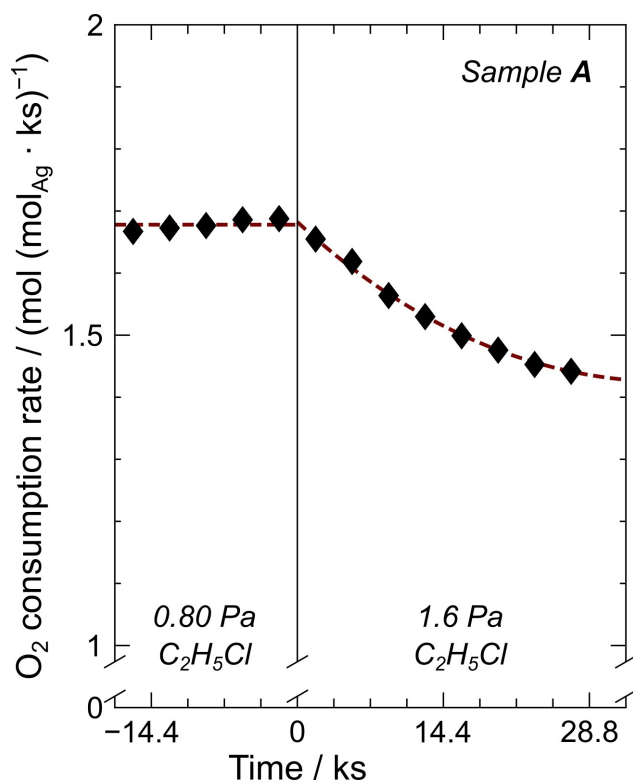
ChemCatChem

Research Article
doi.org/10.1002/cctc.202301369

**Chemistry
Europe**
European Chemical
Societies Publishing

Figure 6. Temporal evolution of O_2 consumption rates before ($t < 0$) and after ($t > 0$) increasing C_2H_5Cl pressure at the inlet reactant stream ($t = 0$) from 0.80 to 1.6 Pa during C_2H_4–O_2 reactions on Ag/α-Al$_2$O$_3$ (18 % wt. Ag; Sample **A**, Table 3; 478 K, 110 kPa O_2, 580 kPa C_2H_4, 16 kPa CO_2, 1.6 kPa H_2O, 890 kPa CH_4). The dashed line for $t < 0$ denotes the steady-state rate for 0.80 Pa C_2H_5Cl, and that for $t > 0$ represents an exponential decay, determined via regression of rate versus time data, towards the steady-state rate for 1.6 Pa C_2H_5Cl.

$k_{2\circ}/k_{1\circ}$), as evidenced by the common selectivity versus conversion trends upon changes in C_2H_5Cl concentrations and in extent of deactivation (Figure 4).

C_2H_4–O_2 reactions on Samples **B** (Re), **C** (Cs), and **D** (Re, Cs), which contain one or both promoters (in 380 Ag/Re and Ag/Cs bulk ratios), exhibit prolonged transients upon C_2H_5Cl removal; it requires $> 30,000$ O_2 conversion turnovers to restore rates and selectivities to those for the respective Cl-free samples. Thus, the "irreversible" effects of Cl, shown for the unpromoted catalyst (**A**) in Section 2.3 (Figure 3), are also evident for catalysts containing Cs and Re promoters. These catalysts also exhibit the "reversible" effects of Cl in response to changes in C_2H_5Cl inlet concentrations (Figures 5 and 6). Rates decreased with increasing C_2H_5Cl levels for **B**, **C**, and **D** (Figure 5), and the number of turnovers required to achieve a new steady-state upon increasing C_2H_5Cl pressures (from a non-zero value) is about ten-fold smaller than when removing C_2H_5Cl. These data show that refractory and persistent Cl adlayers also form on Ag surfaces in samples promoted with Cs and Re and that C_2H_4–O_2 reactions occur on landing ensembles present as interstices within such dense adlayers.

O_2 consumption rates on Samples **B**, **C**, and **D** show temperature dependencies similar to those on **A**′ and **A** (Figure 7a). In all cases (except **A**′), these trends reflect the combined effects of temperature on the grouping of parameters that determine first-order O_2 activation rate constants ($k_{1\circ}$, Eq. 5) and on the steady-state coverages of labile Cl adatoms (Cl*) formed at interstices of refractory Cl adlayers; in the case of **A**′, the activation barrier reflects only the effects on $k_{1\circ}$, because of the absence of Cl moderators in these experiments. Such labile Cl* are formed by reactions of C_2H_5Cl (0.80–6.3 Pa) with available landing ensembles; they are removed by reactions between Cl* and hydrocarbons. The relative rates of formation and removal of bound Cl species determine their steady-state coverages during C_2H_4–O_2 reactions. In these experiments, C_2H_4 was used as the predominant Cl scavenger. The pressures of C_2H_4 and CH_4 are comparable, but the empirical response factors (on a molar basis) that multiply the concentrations of each scavenger in empirical relations used to estimate "chloriding effectiveness"[64,65] are about ten-fold larger for C_2H_4 than for CH_4; thus, C_2H_4 is a more effective scavenger of Cl* than CH_4, in spite of its stronger homolytic C–H bonds (465 versus 439 kJ mol^{-1}[66]). These scavenging efficiency factors were confirmed by measurements of Cl* removal rates with C_1–C_4 alkanes and C_2H_4.[62] Taken together, these findings indicate that the kinetically-relevant step for Cl* removal by alkene scavengers is not likely to require the homolytic dissociation of its C–H bonds, the step that limits Cl* removal by alkanes.

O_2 activation rates (per total Ag) on samples containing Re (**B**) or Cs (**C**) are about two-fold lower (for < 2 Pa C_2H_5Cl) than on the unpromoted sample (**A**); the catalyst containing Re and Cs (**D**) showed rates similar to those on the unpromoted sample. The similar temperature trends (activation barriers of (160 ± 10), (120 ± 16), (120 ± 11), and (140 ± 10) kJ mol^{-1}, respectively, for **A**, **B**, **C**, and **D**) and similar trends with C_2H_5Cl pressure (Figure 5) suggest that the introduction of these promoters into Ag/α-Al$_2$O$_3$ using the procedures described in Section 4.1 and their subsequent treatments during "break-in" protocols (described in Section 4.2) do not strongly influence the binding and reactive properties of Ag ensembles on surfaces that contain refractory Cl adlayers, with interstices onto which reactants compete with C_2H_5Cl-derived species that bind reversibly during catalysis. Together, these data suggest that Re and Cs may form domains on Ag surfaces that simply block "landing ensembles" for O_2 activation, but their combined presence may coalesce the two promoters into Re–Cs adducts or as CsRe salts that preferentially segregate at α-Al$_2$O$_3$ surfaces.

The effects of temperature, extent of deactivation, and C_2H_5Cl pressure on selectivity ratios (S_O; Eq. 3) for each of the promoted samples (**B**, **C**, and **D**) are, as for the unpromoted catalyst (**A**, Figure 4), indistinguishable from one another in trends in S_O values with changes in O_2 conversion (X); Figure 7b is analogous to Figure 4 and shows data for all five samples. Thus, the two-parameter model used to describe the selectivity trends on Samples **A**′ and **A** (Eq. 12) also accurately describes the selectivity trends for **B**, **C**, and **D** (Figure 7b), thus allowing any consequences of Re and Cs for selectivity to be expressed in terms of the two rate constant ratios (k_{II}/k_I and $k_{2\circ}/k_{1\circ}$) that determine selectivity in single C_2H_4–O_2 surface sojourns and selectivity losses in secondary EO sojourns. The regressed values of these two parameters are listed in Table 1 together with
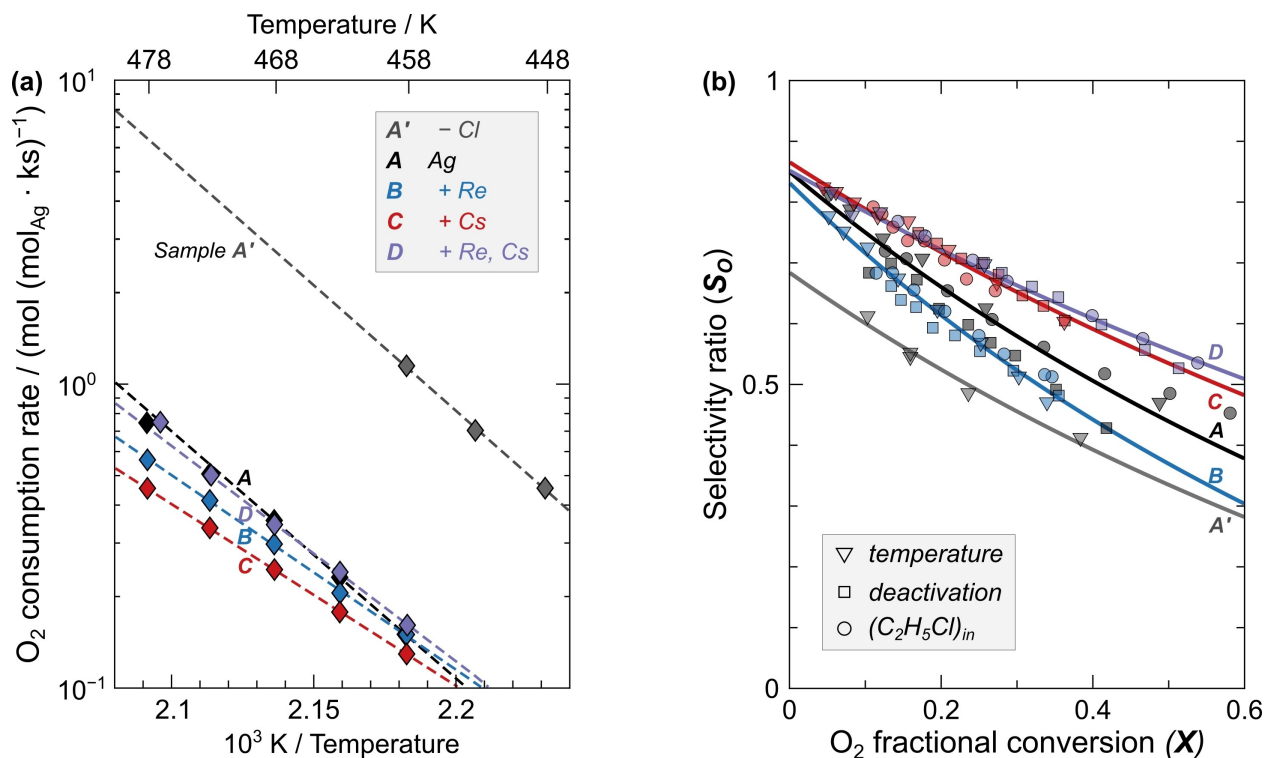
ChemCatChem

Research Article
doi.org/10.1002/cctc.202301369

**Chemistry
Europe**

European Chemical
Societies Publishing

Figure 7. (a) Arrhenius plot of O_2 consumption rates per total Ag (110 kPa O_2, 580 kPa C_2H_4, 16 kPa CO_2, 1.6 kPa H_2O) and (b) selectivity ratios (S_O, Eq. 3) versus O_2 fractional conversion (X) for C_2H_4–O_2 reactions on Ag/α-Al_2O_3 catalysts (18 % wt. Ag) performed in the absence (Sample **A′**, Table 3) and in the presence of C_2H_5Cl (4.0 Pa) with neither Re nor Cs promoters (**A**), with 380:1 Ag:Re (atom ratio; **B**), with 380:1 Ag:Cs (**C**), and with both Re and Cs (380:1 each; **D**). The dashed lines in (a) represent those of best fit determined via linear regression on a semilogarithmic scale for temperatures below 470 K, and the solid lines in (b) are model predictions made using best fit parameters (Table 1) determined via non-linear regression of data to the functional form of Equation 12. For (b), the triangles, squares, and circles denote data in which X was varied by changing, respectively, temperature (433–493 K; 110 kPa O_2, 4.0 Pa C_2H_5Cl), extent of deactivation (473 K, 64 kPa O_2, 4.0 Pa C_2H_5Cl), and inlet C_2H_5Cl pressure (0.80–6.3 Pa; 478 K, 110 kPa O_2). In all experiments, the C_2H_4:O_2 ratio was 5.2, 16 kPa CO_2 and 1.6 kPa H_2O was added to reactant streams, and the total pressure was 1600 kPa, such that the CH_4 pressure was either 1200 or 890 kPa.

measured O_2 consumption rates (per total Ag) in each sample (at 453 K and 478 K). The solid curves in Figure 7b reflect model predictions (Eq. 12) using the best fit parameters.

At the conditions of these experiments, Re and Cs promoters, whether present together or as individual components, do not influence primary selectivity-determining rate constant ratios (k_{II}/k_I; Table 1), as also shown by their similar asymptotic selectivities at low O_2 conversions (Figure 7b). This shows that the Re and Cs moieties (or Re–Cs mixed species) that ultimately form on Ag (and/or α-Al_2O_3) surfaces through the synthesis and "break-in" protocols used here (Sections 4.1 and 4.2) do not affect the ratios of intrinsic rate constants for the elementary steps at primary selectivity-determining branch points, which occur upon O_2 activation at landing ensembles to form O_2* and upon formation of a bound precursor to EO (EO*) on Ag surfaces with refractory Cl adlayers. The relative likelihood that O_2* undergoes (O—O)* bond cleavage (Step II(b) in Scheme 3) versus engaging with C_2H_4 in electrophilic epoxidation (Step I(a)) is not altered by the promoters, and they also do not change the ratio of intrinsic rate constants for the bimolecular surface reaction between EO* and nucleophilic O adatoms (Step II(a)) and for EO* desorption (Step I(b)).

These inorganic species, typically denoted as promoters, influence, however, the rate constant ratio that is reflected in

the loss of EO selectivity via secondary combustion reactions ($k_{2°}/k_{1°}$). Re incorporation via impregnation of $NH_4ReO_4(aq)$ solutions into Ag/α-Al_2O_3 (Sample **B**) leads to a higher $k_{2°}/k_{1°}$ value than on the Re-free version of this catalyst (**A**; 1.6 versus 1.3; Table 1). This reflects an increase in the number of acid centers (ρ_{acid} in Eq. 6), which catalyze EO isomerization and hydrolysis (Reaction IV; Scheme 1); these reactions form CH_3CHO and $(CH_2OH)_2$, respectively (together denoted as $\mathcal{I}$ in Scheme 1). Apparent first-order rate constants for combustion of CH_3CHO (3.0 Pa) and $(CH_2OH)_2$ (1.9 Pa) were measured to be 30- and 300-fold higher, respectively, than that for EO (500 Pa) on 41 % wt. Ag/α-Al_2O_3 at 523 K,[8] a trend that likely reflects the C—H bond dissociation energies within the oxygenate substrates (394, 385, and 421 kJ mol^{-1} for CH_3CHO (a number-weighted average of aldehydic (374 kJ mol^{-1}) and α-C–H (394 kJ mol^{-1}) bonds), $(CH_2OH)_2$, and EO, respectively), since oxidation cascades are initiated by H-abstraction. These species are seldom detected in product streams[8–12,14–17,26,33,67] and when detected correspond to selectivities below 0.1 % CH_3CHO and with yields that remain constant with changes in residence time.[12] This indicates that $\mathcal{I}$ can be treated as a reactive intermediate present at pseudo steady-state concentrations, such that higher ρ_{acid} values lead to higher EO combustion (Reactions IV and V). The number of Lewis acid sites on Al_2O_3-

ChemCatChem

Research Article
doi.org/10.1002/cctc.202301369

**Chemistry
Europe**
European Chemical
Societies Publishing

supported ReO$_x$ clusters have been shown to increase as the Re content increases in ReO$_x$/γ-Al$_2$O$_3$ samples prepared via impregnation with HReO$_4$(aq) from infrared spectra of samples dosed with pyridine at ambient temperature and evacuated *in vacuo* at 473 K.[68] This is consistent with the inference that Re species introduced via contact with perrhenate solutions leads to higher densities of acid sites, likely to reside at support surfaces. Alkali metals are known to neutralize acid sites on Al$_2$O$_3$ surfaces;[69] a previous study showed that CH$_3$CHO isomerization rates on Ag/α-Al$_2$O$_3$ (0.83%wt. Ag, 78 m^{2}g^{-1}) are inhibited by Cs addition (0.46:1 Ag:Cs).[70] Such effects are reflected here in the lower $k_{2°}/k_{1°}$ ratios measured after Cs addition to the unpromoted Ag/α-Al$_2$O$_3$ sample (1.0 versus 1.3 for Samples **C** versus **A**, respectively; Table 1). The $k_{2°}/k_{1°}$ ratio is also lower for the sample involving both Re and Cs (0.89 for **D**) compared to both the unpromoted (1.3 for **A**) and Re-containing samples (1.6 for **B**), showing that Cs can also neutralize the additional acid sites that are formed upon incorporating Re (**B**).

These data show that the predominant consequences of Re and Cs, at the conditions, catalysts, and treatment protocols used here, are on the rates of reactions of EO after its formation on Ag surfaces and reflect the formation (by Re) and the titration (by Cs) of acid sites and not on the number or nature of the Ag surfaces involved in kinetically-relevant O$_2$ activation steps involved in EO synthesis and primary combustion reactions. These observations do not contradict inferences from state-of-the-art EO synthesis catalysts of higher EO selectivities (even above the monooxygenase limit; > 0.857 C-basis or, equivalently, S_O > 1) when Re and Cs are present as promoters. These results demonstrate, however, that the presence of these promoters is required, but not sufficient, for such selectivity enhancements and that the placement of such species through treatment and reaction protocols contributes to their efficacy as selectivity enhancers through mechanisms that have remained controversial decades after the discovery of these promotional effects. The weak effects of Re and Cs on O$_2$ activation rates and the rate constant ratio that determines selectivity in primary C$_2$H$_4$—O$_2$ sojourns (k_{II}/k_I) stand in stark contrast to the "irreversible" effects of Cl (Section 2.3).

The next Section demonstrates the formation of refractory O adlayers on Ag surfaces through transient reactions of N$_2$O. Such surface passivation weakens O* binding to allow for recombinative desorption and steady-state N$_2$O decomposition catalysis, which likely proceeds through the same O* and O$_2$* intermediates encountered in C$_2$H$_4$—O$_2$ reactions. These O$_2$-derived species bind at landing ensembles formed as interstices of the O adlayer. The ensembles become smaller in size and fewer in number when the refractory adlayer comprises both O* and Cl*, which further prevents O$_2$* dissociation and preserves more electrophilic O-atoms for C$_2$H$_4$ epoxidation.

2.5. Formation of refractory O- and Cl-adlayers and their consequences on O-atom addition rates

This Section examines the binding and reactivity of O species at Ag surfaces to probe the effects of Cl on C$_2$H$_4$—O$_2$ reaction rates and selectivity. These experiments specifically address the formation and presence of refractory adlayers of O and Cl species and of "landing ensembles" within their interstices; such restricted spaces can prevent O$_2$ dissociation to form nucleophilic O* atoms (Step II(b), Scheme 3) that bypass the direct use of the electrophilic O-atom in O$_2$* (Step I(a) and I(b)), but also weaken the binding of O$_2$-derived bound species to allow the completion of EO formation turnovers. This inquiry utilizes N$_2$O to measure rates of O-atom addition onto Ag particles. N$_2$O, though seemingly less relevant to EO synthesis compared to O$_2$, is useful as a source of O-atoms because it allows the stoichiometric delivery of single O-atoms:

$$N_2O + {}^* \rightarrow N_2 + O^* \tag{13}$$

but ultimately allows their recombinative desorption as O* coverage increases and repulsive interactions weaken O* binding, thus enabling catalytic N$_2$O decomposition turnovers:

$$2N_2O \rightarrow 2N_2 + O_2 \tag{14}$$

Accurate assessments of O-atom addition rates using O$_2$ rely on precise measurements of small differences in O$_2$ concentration between reactor inlet and exit streams, and even with such precision, O$_2$ disappearance rates may not reflect O-atom addition (i.e., O* formation), but instead the formation of bound dioxygen intermediates (e.g., O$_2$*).

O-atom addition reactions were conducted with Ag/α-Al$_2$O$_3$ (18%wt. Ag) in its "fresh" form after its synthesis (described in Section 4.1; ⟨d_{SEM}⟩ = 140 nm, Đ=0.0084, Figure 2) and aliquots of this catalyst after C$_2$H$_4$—O$_2$ reactions in the absence and presence of C$_2$H$_5$Cl (Samples **A′** (240 nm, Đ=0.0049) and **A** (310 nm, Đ=0.0038), respectively); the procedure used to extract samples from reactors is described in Section 4.2, and the C$_2$H$_4$—O$_2$ conditions used for **A′** and **A** are detailed in the captions of Figures 1, 4, and 7. All samples were treated by sequential contact with O$_2$ (4.0 kPa, 1.8 ks), inert (He, 1.8 ks), CO (1.0 kPa, 7.2 ks), and inert (1.8 ks) flowing streams at 548 K to remove labile species and to form "essentially bare" Ag nanoparticles and then exposed to an N$_2$O-containing stream (1.0 kPa; He balance) at 548 K.

The dash-dotted (− · −) and dotted (···) traces in Figure 8a show, respectively, N$_2$ and O$_2$ formation rates as a function of the time elapsed from initial contact with N$_2$O on the "fresh" form of the Ag/α-Al$_2$O$_3$ (18%wt. Ag) sample (denoted here as **A″**). N$_2$ evolution rates decreased and O$_2$ evolution rates increased with time, reaching the molar N$_2$/O$_2$ ratio of 2 expected for catalytic decomposition (Eq. 14). The molar N$_2$/O$_2$ ratios in the effluent stream being initially larger than 2 is indicative of the irreversible binding of O* species (Eq. 13), which ultimately reach a coverage and reactivity that allows their recombinative desorption to proceed at rates equal to those at which they form, leading to steady-state N$_2$O decomposition turnovers (and to N$_2$/O$_2$ ratios of 2). O-atom addition rates (r_{O*}) can be assessed from this initial imbalance in N$_2$ (r_{N_2}) and O$_2$ (r_{O_2}) evolution rates:
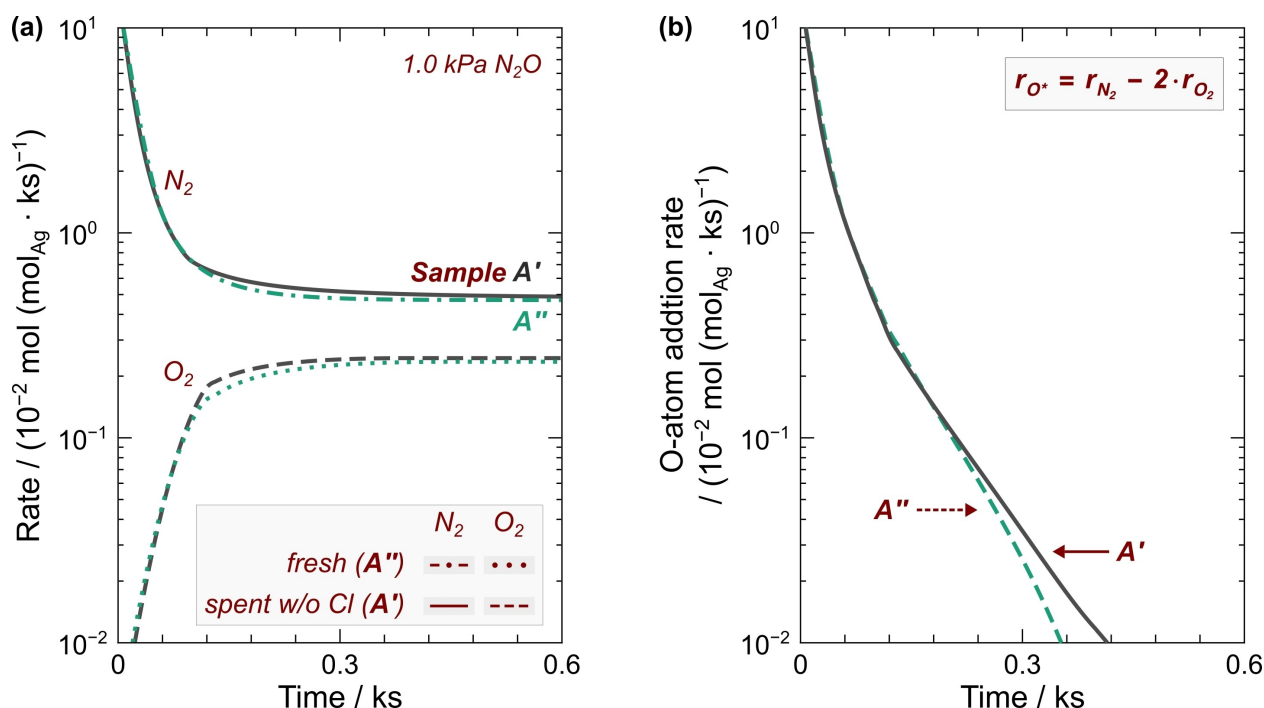
ChemCatChem

Research Article
doi.org/10.1002/cctc.202301369

**Chemistry
Europe**
European Chemical
Societies Publishing

Figure 8. (a) N_2 and O_2 formation and (b) O-atom addition rates (r_{O^*}; Eq. 15), per total Ag, upon contacting Ag/α-Al$_2$O$_3$ (18 % wt. Ag) samples with a N_2O (1.0 kPa) stream at 548 K. The dash-dotted (N_2) and dotted (O_2) curves in (a) and the dashed curve in (b) correspond to the reaction with the "fresh" Ag/α-Al$_2$O$_3$ sample (**A″**), while the solid (N_2) and dashed (O_2) curves in (a) and the solid curve in (b) are for the "spent" sample collected after C$_2$H$_4$–O$_2$ reactions in the absence of C$_2$H$_5$Cl (**A′**). Prior to N_2O exposure, samples were subjected to successive oxidative (4.0 kPa O$_2$) and reductive (1.0 kPa CO) treatments at 548 K.

$$r_{O^*}(t) = r_{N_2}(t) - \left[2 \cdot r_{O_2}(t) \right] \qquad (15)$$

The dashed (---) curve in Figure 8b shows r_{O^*} versus time for the fresh sample (**A″**). The number of bound O-atoms stranded at each point in time ($N_{O^*}(t)$) can be calculated by integrating the r_{O^*} versus t curve:

$$N_{O^*}(t) = \int_0^t r_{O^*}(t') \, dt' \qquad (16)$$

For **A″**, the asymptotic total number of bound O-atoms before steady-state catalysis ($N_{O^*}^\infty = N_{O^*}(t \to \infty)$) is 0.0034 O-atoms per Ag atom, a value that is smaller than the SEM-derived estimates of the fraction of the Ag atoms exposed at particle surfaces (Đ = 0.0084; Figure 2).

N_2O decomposition rates reach steady-state values only after the formation of an O adlayer that weakens the binding of O adatoms, decreases the mean distance among O* species, and thus increases the rates of bimolecular recombinative desorption events. These data are consistent with the observed decrease in isosteric heats of O adsorption with increasing O* coverage,[71] specifically, from 175 to 74 kJ mol^{-1} as coverage increased from 0.17 to 0.33 of a monolayer on polycrystalline Ag powders.[71] These heat values were assessed from uptakes measured gravimetrically by dosing samples, which were subjected to > 20 cycles of oxidation (1.3 kPa O$_2$) and reduction (1.3 kPa CO or 1.3 kPa H$_2$) at > 563 K to obtain reproducible uptake isotherms, with known amounts of O$_2$ at 451–612 K. At low coverages, dissociative O$_2$ adsorption on Ag is exothermic,

and the lower bound for the activation barrier for the microscopic reverse process, recombinative desorption, corresponds to barrierless adsorption and is equal to twice the heat of O adsorption. For the Ag particles examined here (**A″**, Figure 8), this kinetic hurdle remains too high such that O$_2$ evolution rates cannot keep up with those for stoichiometric N_2O decomposition until the formation of a refractory O adlayer (with a saturation O*/Ag molar ratio of 0.0034), which dampens the hurdle to allow for the two rates to match and for steady-state catalysis to be realized.

The temporal N_2 and O_2 evolution (Figure 8a) and O-atom addition (Figure 8b; r_{O^*}, Eq. 15) rate profiles for the fresh form (**A″**) are, within experimental error, indistinguishable from those for the "spent" sample collected after C$_2$H$_4$–O$_2$ reactions in the absence of C$_2$H$_5$Cl (**A′**; solid (—) and dashed (---) curves for, respectively, N_2 and O_2 in Figure 8a and the solid curve for r_{O^*} in Figure 8b), resulting in closely matching $N_{O^*}^\infty$ values (0.0034 and 0.0033 for **A″** and **A′**, respectively). These similarities in reactivity and number of O* species emerge despite the 1.7-fold difference in estimates of fractional dispersion from SEM (Figure 2; 0.0084 and 0.0049 for, respectively, **A″** and **A′**). SEM data were collected on samples treated in N_2 flow at 563 K for **A″** (Section 4.1) and after C$_2$H$_4$–O$_2$ reactions (> 200 h) and extraction from the reactor (Section 4.2) for **A′**; they reflect samples that are likely to have different forms of Ag: essentially bare and reduced Ag particles for **A″** and those with a passivating layer of O adatoms, along with other debris which may have accumulated during the C$_2$H$_4$–O$_2$ reactions, for **A′**. In contrast, treatments before the N_2O probe reactions sought to

restore (for both samples) a common form of reduced Ag nanoparticles through sequential treatments at 548 K in oxidative (4.0 kPa O_2) and reductive (1.0 kPa CO) environments. The nearly identical transient and catalytic N_2O decomposition rates show that the applied treatment removes any residues formed during the C_2H_4–O_2 reactions (for **A′**) and establishes the binding and reactive properties of O* for the Ag particles within **A″** and **A′** to be the same.

Scheme 4 depicts a schematic for the evolution of bound species on Ag surfaces upon exposure to N_2O. The initial treatments form a surface that is essentially bare but start to accumulate "permanent" O* species ($\mathbf{\Omega}$*=O*). O_2 evolution reaches constant rates (and steady-state catalysis becomes the prevalent mode of N_2O decomposition) upon completion of a surface mosaic composed of a refractory adlayer and intralayer "landing ensembles" onto which N_2O can dissociate. The O* species at the interstices are labile compared to those comprising the adlayer, since the former are destabilized by inter-atom repulsion imposed by the mosaic, thus favoring their recombinative desorption and the completion of catalytic turnovers. Such cycles at interstices are likely to involve the types of O_2* and O* species prevalent during O_2 chemisorption events that mediate selective and unselective C_2H_4–O_2 reactions via the use of electrophilic and nucleophilic O-atoms. The O* species formed from N_2O can recombine with other interstitial O* species via facile steps, but also occasionally react with an O* in the refractory adlayer, leading to the formation of larger ensembles that are readily titrated by a fast stoichiometric N_2O decomposition event in these experiments. A similar process that leads to the occasional local removal of O* atoms from the refractory adlayer (via recombinative desorption or reaction with reductants) during C_2H_4–O_2 reactions would bring significant consequences to EO selectivities; in this case, the local and occasional formation of such larger ensembles opens channels for the dissociation of O_2* to form two nucleophilic O* species (Steps II(b) in Scheme 3), thus precluding the use of the electrophilic O-atom in O_2* for EO formation events (Steps I(a) and (b)).

The weakening of O* binding with increasing O* coverage[71] is evident in the observed changes in stoichiometric N_2O decomposition rates as the reaction forms O* and its coverage increases with time (Figure 8b). These rates would be expected to remain proportional to the number of remaining unoccupied spaces if the binding properties of such ensembles remain unchanged as they become less prevalent with increasing O* coverages. Such uniform binding and reactive properties would manifest as a straight line in the semilogarithmic plot of O-atom addition (r_O*, Eq. 15) versus time (Figure 8b); the observed non-linearity reflects the nonuniformity. A rate constant (k_{app}^{O*}) for the formation of O* in the refractory adlayer can be defined as the rate at which O* forms at each point in time (per total Ag; r_O*, Eq. 15) divided by the number of binding spaces within the adlayer that is not yet occupied (calculated from the saturation O*/Ag ratios; Eq. 16; N_O^{∞}* = 0.0033 (mol O*) (mol total Ag)$^{-1}$ for Sample **A′**; Figure 8b, solid):

$$k_{app}^{O*}(t) = \frac{r_O*(t)}{N_\Omega^{\infty}* \;-\; N_\Omega*(t)} \tag{17}$$

Here, for Sample **A′**, the refractory adlayer only comprises O* ($\mathbf{\Omega}$*=O*). The apparent rate constant decreases with increasing O* coverage, as shown in Figure 9b (triangles), where the abscissa values represent the fraction of spaces within the adlayer not yet filled by O* at each time during the transient stoichiometric N_2O decomposition: $(1 - N_O*(t)/N_O^{\infty}*)$. The value of k_{app}^{O*} decreases about seven-fold between the bare surface and the O* coverage at which catalytic N_2O decomposition rates reach steady-state. This implies that the N_2O decomposition transition state (TS), which requires binding to an ensemble within the adlayer, becomes increasingly destabilized with increasing adlayer density, a consequence of the same repulsive interactions that lead to the weaker O* binding that allow for their desorption. The calculated k_{app}^{O} values for the "fresh" sample (**A″**) are nearly identical to those for the sample collected after C_2H_4–O_2 reactions in the absence of C_2H_5Cl (**A′**), since the oxidation-reduction treatment that was applied prior to the N_2O reaction restores the "spent" sample to a form with a number of "landing ensembles" and with binding and reactivity properties thereof for O* that are the same as in the "fresh" sample.

The exposure of the Ag/α-Al_2O_3 sample to C_2H_5Cl moderators during C_2H_4–O_2 reactions led to a nearly ten-fold decrease in O_2 consumption rates (per total Ag; Sample **A** versus **A′**; Figures 1 and 3 and Table 1) but did not significantly alter the activation barrier ((160 ± 10) versus (170 ± 6) kJ mol^{-1} for, respectively, **A** and **A′**), indicative of a change to the number but
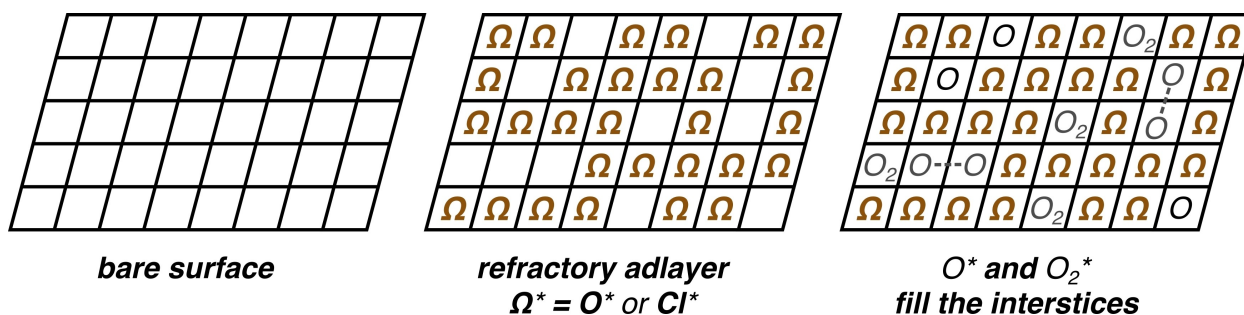
Scheme 4. Strongly bound O and Cl adatoms ($\mathbf{\Omega}$*, $\mathbf{\Omega}$*=O* or Cl*) accumulate on Ag surfaces to form a refractory adlayer. Labile O adatoms and bound dioxygen species (O_2*) fill in the available spaces at the interstices.
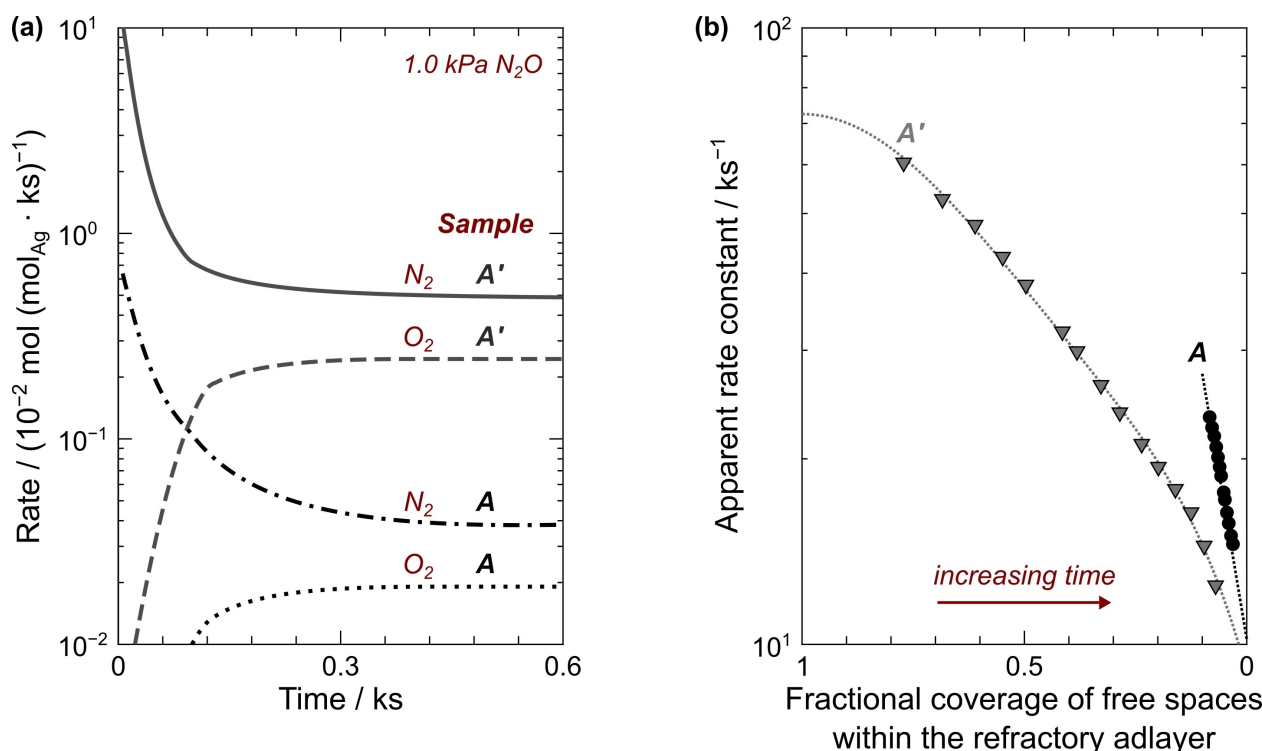
ChemCatChem

Research Article
doi.org/10.1002/cctc.202301369

Chemistry Europe
European Chemical
Societies Publishing

Figure 9. (a) N_2 and O_2 formation rates, per total Ag, upon contacting Ag/α-Al$_2$O$_3$ (18 wt. Ag) samples with a N_2O (1.0 kPa) stream at 548 K. The solid (N_2) & dashed (O_2) curves and the dash-dotted (N_2) & dotted (O_2) curves correspond to data for samples retrieved after C_2H_4–O_2 reactions in the absence (**A'**) and presence (**A**), respectively, of C_2H_5Cl. (b) Apparent rate constants for stoichiometric N_2O decomposition (k_{app}^O; Eq. 17) versus fractional coverage of unoccupied interstices within refractory adlayers comprising O* for Sample **A'** (triangles) and both O* and Cl* for Sample **A** (circles); the dotted curves are visual guides.

not the intrinsic reactivity of site ensembles for O_2 activation. The treatments in oxidative (4.0 kPa O_2, 1.8 ks) and reductive (1.0 kPa CO, 7.2 ks) environments at 548 K used before the N_2O tests appear to remove any residues present during C_2H_4–O_2 reactions on samples not exposed to Cl (Figure 8), since the N_2 and O_2 evolution rates, and the O* formation rates calculated therefrom (r_O*; Eq. 15), are indistinguishable between the "fresh" sample (**A''**) and the treated "spent" sample without Cl (**A'**). The sample exposed to C_2H_5Cl during C_2H_4–O_2 reactions (**A**), despite being subjected to the same treatment in oxidative and reductive environments, also show much lower rates of N_2 and O_2 formation (per total Ag) during stoichiometric N_2O decomposition (1.0 kPa, 548 K) and of steady-state catalytic decomposition rates after the formation of a refractory O* adlayer that passivates such surfaces (Figure 9a; dash-dotted (N_2) and dotted (O_2) traces for **A** versus solid (N_2) and dashed (O_2) traces for **A'**); the initial and steady-state N_2 formation rates are 19- and 13-fold lower for **A** versus **A'**. The amount of O* deposited during the approach to the catalytic steady-state is also about 10-fold smaller (saturation O*/Ag ratios of $3.2 \cdot 10^{-4}$ (**A**) and $3.3 \cdot 10^{-3}$ (**A'**)), implying that species derived from C_2H_5Cl occupy spaces in the refractory adlayer that would otherwise be occupied by O* and that such Cl-containing species persist on Ag surfaces during N_2O and C_2H_4–O_2 reactions, extraction of samples from the reactor (Section 4.2), and treatment in sequentially O_2 (4.0 kPa) and then in CO (1.0 kPa) at 548 K.

These data together show that Cl species form a refractory adlayer that is more persistent than those derived only from O_2,

as evident from treatments that restore Ag surfaces to their fresh state in Sample **A'** (Figure 8) but not **A** (Figure 9) and from the slow recovery of O_2 consumption rates upon removal of C_2H_5Cl from reactant streams during C_2H_4–O_2 reactions (Figure 3). The similar (ten-fold) decreases to stoichiometric O* coverages, transient N_2O decomposition rates, and catalytic transformations of N_2O and C_2H_4–O_2 reactants demonstrate that the refractory adlayer becomes denser when it comprises both Cl* and O* instead of solely O*. In the presence of Cl*, the interstitial site ensembles that bind labile O* and evolve and activate O_2 to turnover for N_2O decomposition and aerobic C_2H_4 oxidation become fewer in number and smaller in size.

The calculation of apparent O-atom addition rate constants during transient measurements (k_{app}^O; Eq. 17) requires an assessment for the numbers of adatoms deposited onto Ag surfaces before exposure to N_2O and at the onset of steady-state catalytic decomposition reactions (N_Ω^∞* in Eq. 16). These numbers are straightforward to assess for the reaction on Sample **A'** (without Cl*; Figure 9b, triangles): the initial coverage is zero and the N_Ω^∞* value is equal to the saturation O*/Ag ratio ($3.3 \cdot 10^{-3}$); these values correspond to fractional coverages of free spaces within the refractory adlayer (i.e., the abscissa values in Figure 9b) of unity and zero. For Sample **A** (with Cl*; Figure 9b, circles), the initial coverage of free spaces is non-zero, since some are already occupied by the persistent Cl adatoms. The k_{app}^O values for the Cl-containing sample were estimated by presuming that the number of total spaces within the Cl* and O* adlayer for **A** is identical to that for the O*

ChemCatChem

Research Article
doi.org/10.1002/cctc.202301369

Chemistry
Europe

European Chemical
Societies Publishing

adlayer for **A′** ($N_{\Omega}^{\infty}* = 3.3 \cdot 10^{-3}$) and that the difference between the saturation O*/Ag ratios for **A′** ($3.3 \cdot 10^{-3}$) and **A** ($3.2 \cdot 10^{-4}$) is equal to the number of spaces initially occupied by Cl*. Thus, the abscissa values in Figure 9b for Sample **A** span from 0.097 ($= 0.00032/0.0033$) to zero.

The refractory adlayer imparts inter-atom repulsive forces that weaken O* binding, enable O* recombinative desorption, and impede O* deposition, leading to steady-state turnover of interstitial site ensembles for N$_2$O decomposition. The prevalence of these repulsive forces manifests here as $k_{app}^{O}*$ values that decrease with increasing occupancy of spaces within the refractory adlayer (Figure 9), a reflection of N$_2$O decomposition transition states that become increasing destabilized as mean distances between O*/Cl* species within the adlayer decreases. These $k_{app}^{O}*$ values are slightly larger (by, at most, a factor of 1.7) when the refractory adlayer contains Cl* (**A** (circles) versus **A′** (triangles), Figure 9b), which implies that the N$_2$O decomposition TS is destabilized to a lesser extent when the intralayer site ensemble is surrounded by Cl* instead of O*. The reduced repulsion between bound species on Cl-containing Ag surfaces may contribute in effecting higher primary selectivities in C$_2$H$_4$–O$_2$ reactions (smaller k_{II}/k_I values for Sample **A** versus **A′**, Table 1) if the transitions states for the two bimolecular surface reactions that lead to loss of electrophilic O-atoms (reaction between bound precursors to EO (EO*) and O* and O$_2$* dissociation; Steps II(a) and II(b), respectively, in Scheme 3) are destabilized to a greater extent by the refractory adlayer than those for the two desired reactions (direct epoxidation of C$_2$H$_4$ by O$_2$* and EO* desorption; Steps I(a) and Step I(b), respectively) which only involve one bound species.

Next, the consequences of refractory adlayers and their composition on the distribution and reactivity of O$_2$-derived species at inter and intralayer landing ensembles are examined through O-removal reactions using CO. These experiments provide further evidence that the isolation of small site ensembles within the mosaic of strongly bound O* and Cl* species prevents O$_2$* dissociation and that this prevention is what allows electrophilic O-atoms to be utilized such that EO selectivities approach the monooxygenase limit (Figures 4 and 7b).

2.6. Formation of isolated landing ensembles at interstices of refractory adlayers that bind O$_2$ and inhibit its dissociation

The bare and reduced surfaces of Ag nanoparticles within the as-prepared Ag/α-Al$_2$O$_3$ sample (Sample **A″**) accumulate O adatoms (O*) upon contacting them with a dilute N$_2$O stream (1.0 kPa) at 548 K. O$_2$ evolves via recombinative O* desorption only when the surfaces are sufficiently passivated and O* binding energies sufficiently weakened by inter-atom repulsive forces. The number of O* species within the passivating refractory O adlayer is equal to 0.0034 mol O per total Ag. In an inert environment, these strongly bound O adatoms are not expected to recombine and desorb when holding at the temperature (548 K) at which they were accumulated. They are expected, however, to be removed by CO, since the sequential

oxidative (4.0 kPa O$_2$) and reductive (1.0 kPa CO) treatments at 548 K give N$_2$ and O$_2$ evolution (Figure 8a) and O* formation (Figure 8b) profiles for the "spent" Ag/α-Al$_2$O$_3$ sample (retrieved after C$_2$H$_4$–O$_2$ reactions in the absence of C$_2$H$_5$Cl; Sample **A′**) that are indistinguishable from those for the "fresh" sample, indicative of the efficacy of CO to remove O* that may accumulate in oxidative treatments under either O$_2$ or N$_2$O.

The left panel of Figure 10a shows O-atom addition rates (r_O*; Eq. 15) for the N$_2$O reaction (1.0 kPa, 548 K) on the "spent" sample collected after C$_2$H$_4$–O$_2$ reactions in the absence of C$_2$H$_5$Cl (Sample **A′**); these data are the same as the solid trace in Figure 8b. After 0.6 ks of exposure to N$_2$O, which, for **A′**, deposits 0.0033 mol O per total Ag, N$_2$O was removed, and the sample was purged in flowing inert (He) at the same temperature (548 K) for 1.8 ks. This would allow for the desorption of any N$_2$O-derived species bound at interstices of the refractory adlayer but not for the recombinative desorption of O adatoms that comprise it. The inlet stream was then switched to CO (1.0 kPa), and the right panel in Figure 10a shows CO$_2$ formation rates versus time elapsed after the He/CO switch. The O-removal rate decreases monotonically with increasing reaction time, and the total amount of CO$_2$ formed after 3.6 ks (0.0032 mol CO$_2$ per total Ag) is in excellent agreement with the total amount of O deposited in the N$_2$O reaction (left panel, 0.0033 mol O per total Ag). This result is consistent with the expectation that CO at 548 K can remove the O* species that constitute the refractory adlayer and are recalcitrant towards recombinative desorption.

The observed non-linearity in the semilogarithmic rate versus time curves for both the formation and removal (left and right panels, respectively, of Figure 10a) of the refractory O adlayer are manifestations of the non-uniformity in O* binding. Previous thermodynamic measurements of O uptake on polycrystalline Ag powders[71] showed that isosteric heats of oxygen adsorption decreased by approximately 100 kJ mol^{-1} as the O* coverage increased approximately two-fold (from 0.17 to 0.33); at 548 K, this would correspond to a ten-decade decrease in the binding constant (an estimate based on isosteric binding entropies being invariant with coverage). Apparent rate constants for O-removal by CO to form CO$_2$ ($k_{app}^{CO_2}$) can be calculated in a manner analogous to those for O-addition by N$_2$O ($k_{app}^{O}*$; Eq. 17):

$$N*(t) = \int_0^t r_{CO_2}(t') \, dt' \tag{18}$$

$$k_{app}^{CO_2}(t) = \frac{r_{CO_2}(t)}{N_{\Omega}^{\infty}* - N*(t)} \tag{19}$$

where $r_{CO_2}(t)$ and $N*(t)$ are the CO$_2$ formation rate and the number of free spaces within the refractory adlayer (both normalized to the total amount of Ag in the sample) at each point in time and $N_{\Omega}^{\infty}*$ still represents the total number of spaces within the adlayer (taken as the saturation O*/Ag ratio: 0.0033). The triangles and squares in Figure 10b represent values of $k_{app}^{O}*$ (Eq. 17), which are the same as those in Figure 9b, and $k_{app}^{CO_2}$ (Eq. 19), respectively; the former spans approximately
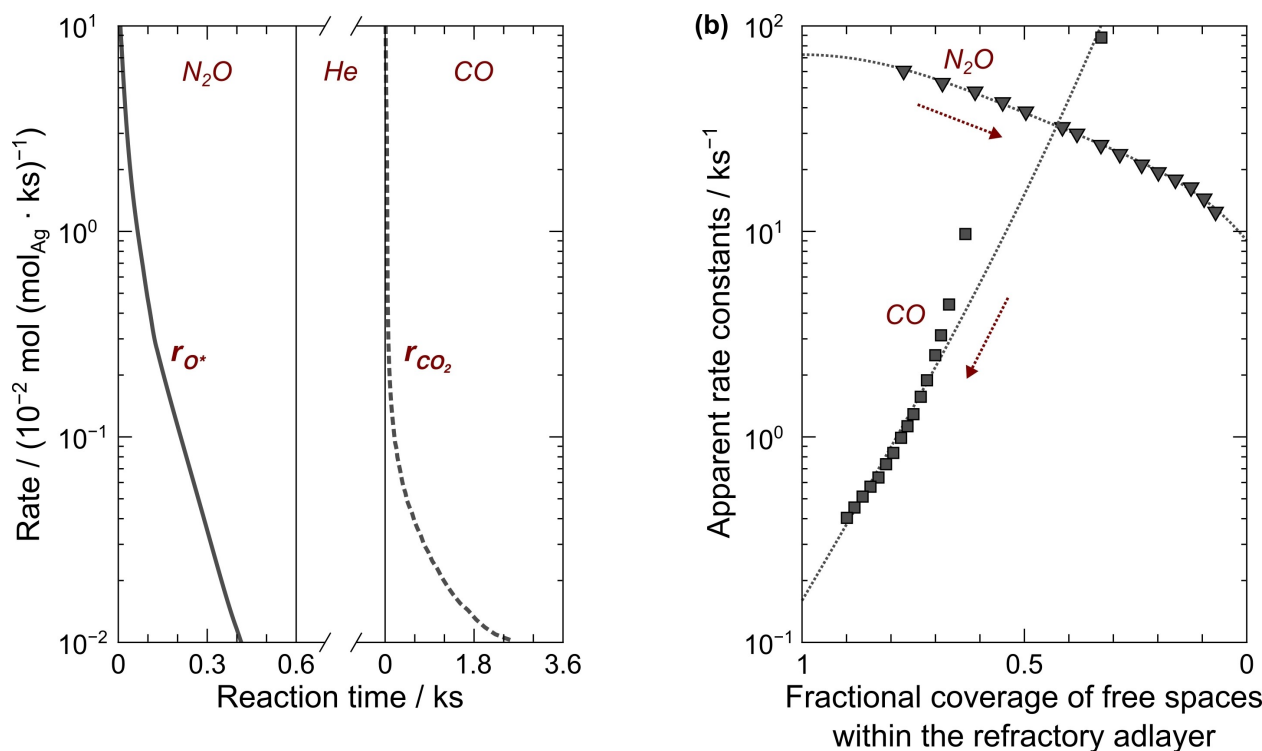
ChemCatChem

Research Article
doi.org/10.1002/cctc.202301369

Chemistry
Europe
European Chemical
Societies Publishing

Figure 10. (a) (*left panel*) Rates of O adatom formation (Eq. 15) upon contacting the "spent" Ag/α-Al$_2$O$_3$ (18 % wt. Ag) sample retrieved after C$_2$H$_4$–O$_2$ reactions in the absence of C$_2$H$_5$Cl (Sample **A′**; Table 3) with a N$_2$O (1.0 kPa) stream at 548 K; prior to N$_2$O exposure, samples were treated at 548 K in, sequentially, oxidative (4.0 kPa O$_2$, 1.8 ks) and reductive (1.0 kPa CO, 7.2 ks) environments. (*right panel*) Rates of CO$_2$ formation upon contacting the same sample after the N$_2$O reaction (1.0 kPa, 548 K, 0.6 ks) and a subsequent inert purge step (He, 548 K, 1.8 ks) with a CO (1.0 kPa) stream at 548 K. (b) Apparent rate constants for stoichiometric N$_2$O decomposition (triangles, k_{app}^O; Eq. 17) and for stoichiometric O-removal by CO (squares, $k_{app}^{CO_2}$; Eq. 19) versus the fractional coverage of unoccupied spaces within refractory O* adlayers. The dotted curves are visual guides, and the arrows point towards increasing time.

one decade throughout the O-addition reaction while the latter more than three decades. The thermodynamic non-uniformity in O* binding (a difference in binding energy of ~100 kJ mol^{-1}) is more evident in the removal of O* by CO (~30 kJ mol^{-1}) relative to the formation of O* by N$_2$O (~10 kJ mol^{-1}). Both the removal and addition steps are expected to be exergonic, which implies that transition states for both CO$_2$ formation (from CO and O*) and N$_2$O decomposition (to O* and N$_2$) would occur early along their respective reaction coordinates. Thus, the TS for O* removal involves partial cleavage of a Ag–O bond while that for O* addition involves partial cleavage of an O–NO bond, such that the non-uniformity in O* binding (Ag–O formation) is more prominent in the CO reaction than for the N$_2$O reaction.

C$_2$H$_4$–O$_2$ and N$_2$O decomposition catalysis likely proceeds through labile O$_2$* and O* intermediates formed at interstices of refractory adlayers. Such O$_2$* species are expected to exhibit high reactivity in reactions with gas-phase reductants (e.g., C$_2$H$_4$ and CO), since their formation is the rate limiting step in C$_2$H$_4$–O$_2$ reactions (see Section 2.2 for the discussion on the identity of the kinetically-relevant step). Preliminary kinetic data for N$_2$O decomposition catalysis indicates rates as being directly proportional to N$_2$O and inversely dependent on O$_2$, consistent with prevalence of O$_2$-derived species at interstitial landing ensembles. These intermediates are removed during the inert (He) purge that intervenes the isothermal N$_2$O and CO reactions (Figure 10a), and attempts to assess the number and reactivity

of these bound species in isothermal experiments, via transient analysis of rates upon adding or removing one or both reactants during CO-N$_2$O reactions, were unsuccessful because the time scales at which they react at 548 K are much shorter than the temporal resolution of the analysis (~5 s). The number and reactivity of O$_2$-derived species that occupy site ensembles within interstices of the refractory O* adlayer were instead assessed in temperature ramping experiments. Ag/α-Al$_2$O$_3$ samples were subjected to reductive (1.0 kPa CO) and oxidative (4.0 kPa O$_2$) treatments at 548 K, which results in the formation of the refractory adlayer (0.0033 O* per total Ag for Sample **A′**) and filling of the interstitial sites by labile O$_2$-derived species. The samples were then cooled to 233 K in flowing O$_2$ (4.0 kPa) and purged in a flowing inert stream (He, 233 K) before being contacted with a dilute CO (1.0 kPa) stream.

The solid trace in the left panel of Figure 11 shows that CO$_2$ forms readily at 233 K, indicating that surfaces with refractory O* adlayers can retain appreciable coverages of highly reactive O$_2$-derived species that bind to landing ensembles formed at interstices of the adlayers. Such species are likely to include bound dioxygen (O$_2$*), since the dense adlayer imparts inter-atomic repulsion and decreases the size of landing ensembles to prevent O$_2$* dissociation. Previous studies showed that CO reacts with molecularly adsorbed O$_2$ on Ag(110) single crystals at < 100 K;[72,73] in these cases, dissociative adsorption was circumvented by admitting O$_2$ at cryogenic temperatures.
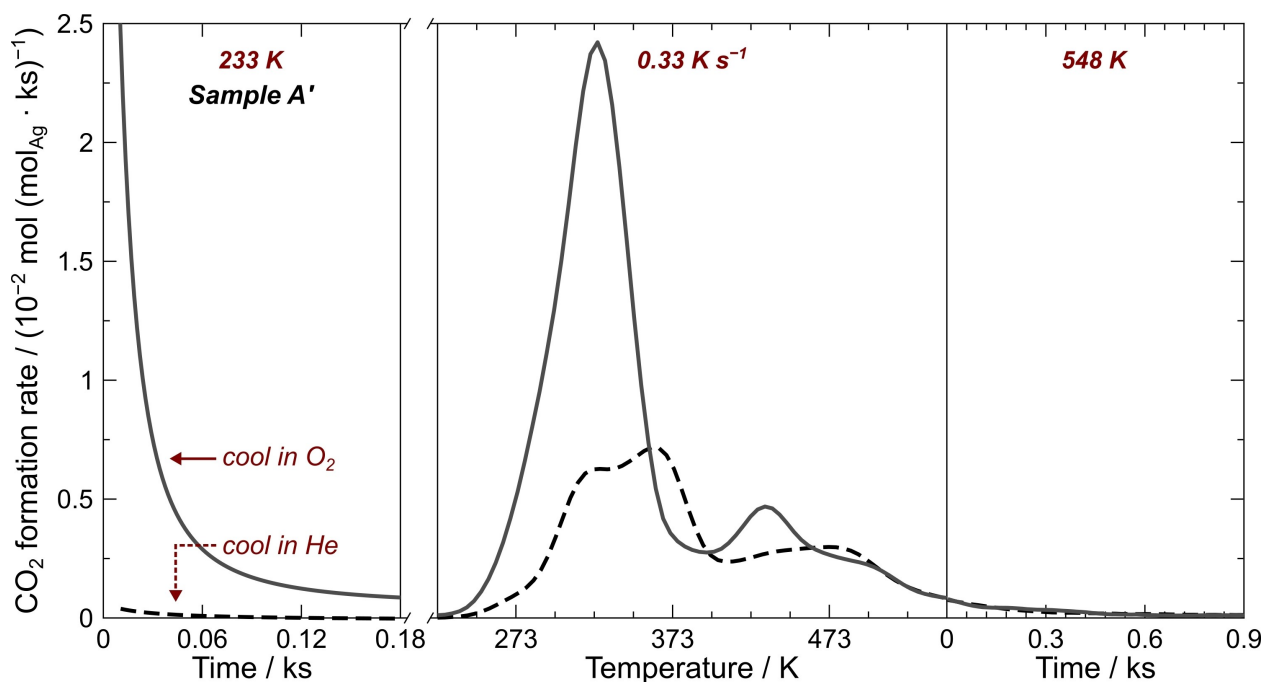
Figure 11. CO_2 formation rates upon contacting the Ag/α-Al_2O_3 (18 %wt. Ag) sample (Sample **A′**; collected after C_2H_4–O_2 reactions in the absence of C_2H_5Cl; Table 3) with a CO (1.0 kPa) stream while holding at 233 K (*left*), then heating at 0.33 K s^{-1} to (*middle*), and holding at (*right*) 548 K. The sample was cooled either in an oxidizing (4.0 kPa O_2, solid) or in an inert (He, dashed) environment upon sequential thermal reductive (1.0 kPa CO, 548 K) and oxidizing (4.0 kPa O_2) treatments at 548 K.

Heating this sample to and then holding at 548 K in flowing CO (1.0 kPa) leads to additional CO_2 being formed; the solid traces in the middle and right panels of Figure 11 show CO_2 rate versus temperature during heating (0.33 K s^{-1}) and time upon holding at the final temperature, respectively. Table 2 lists the amounts of CO_2 formed during the initial isothermal reaction at 233 K, the heating step (233 to 548 K at 0.33 K s^{-1}), and the total amount in all three steps of the experiment (0.0071 O per Ag), which is larger than that corresponding to the refractory adlayer (0.0033 O per Ag). Thus, in addition to the strongly bound O adatoms that comprise the refractory O* adlayer, the oxidative treatment (4.0 kPa O_2) at 548 K and subsequent cooling to 233 K in flowing O_2 (4.0 kPa) forms and retains O_2* and more weakly bound O* species at interstitial site ensembles. The consumption of O_2* by CO to form CO_2 at 233 K leaves behind O*, which binds even more weakly than the labile O* that occupy interstitial sites (instead of O_2*) and the strongly bound O* within the refractory adlayer. The rightmost cartoon in

Scheme 4 depicts the O_2* and labile O* species formed at the interstices of the refractory adlayer.

The dashed traces in Figure 11 represent results from an analogous CO experiment (1.0 kPa CO while holding at 233 K (*left*) and then heating to (0.33 K s^{-1}; *middle*) and holding at (*right*) 548 K) on the same sample (Sample **A′**; Table 3; 18 %wt. Ag/α-Al_2O_3, collected after C_2H_4–O_2 reactions in the absence of C_2H_5Cl) but following a treatment protocol intended to leave behind only the refractory adlayer: the middle cartoon in Scheme 4. This treatment involved the same reductive (1.0 kPa CO) and oxidative (4.0 kPa O_2) treatments as before but with a sweeping inert (He) stream during the subsequent cooling step. After this treatment, only negligible quantities of CO_2 are formed upon contacting the sample with CO (1.0 kPa) at 233 K, and the total amount of CO_2 formed in the subsequent steps of heating to and holding at 548 K (0.0034 CO_2 per Ag; Table 2) is consistent with the amount of O adatoms in the refractory O* adlayer (0.0033 O per Ag). These data show that without O_2

Table 2. Amounts of CO_2 formed (per total Ag) in the three-step CO-mediated O-removal reactions on Ag/α-Al_2O_3 (Samples **A′** and **A**, which were retrieved after C_2H_4–O_2 reactions in the absence and presence, respectively, of C_2H_5Cl; Section 4.2) involving initial isothermal operation at 233 K, heating at 0.33 K s^{-1}, and holding at the final temperature of 548 K (Figures 11 and 12). Samples were subjected to sequential thermal reductive (1.0 kPa CO) and oxidative (4.0 kPa O_2) treatments at 548 K and subsequently cooled in either an oxidizing (4.0 kPa O_2) or inert (He) environment before being contacted with a dilute CO (1.0 kPa) stream.

Sample	Environment in cooling step	CO_2 formed / (10^{-2} mol mol$_{Ag}^{-1}$)		
		233 K	*Heating*	*Total*
A′	4.0 kPa O_2	0.063	0.62	0.71
A′	Inert (He)	<0.003	0.31	0.34
A	4.0 kPa O_2	0.12	0.35	0.56

present in the fluid-phase surrounding the Ag particles the highly reactive O_2^* species, that react with CO at 233 K, and the more labile O^* species, that are removed at lower temperatures (240 K versus 260 K and 330 K versus 370 K for the onsets of and maxima in, respectively, CO_2 formation between the solid and dashed curves, Figure 11), desorb and recombine to evolve O_2 into the sweeping inert stream, leaving behind unoccupied site ensembles within the interstices of the refractory O adlayer.

Refractory Cl^* adlayers are more persistent than those involving only O^*, as reflected by the >10-fold decreases in C_2H_4–O_2 rates (Figures 1, 3, and 7a), stoichiometric and catalytic N_2O decomposition rates (Figure 9), and O^* uptakes (Figure 9). Thus, the number of interstitial landing ensembles that can accommodate highly reactive O_2^* and labile O^* species are fewer in number for Ag surfaces with persistent Cl adatoms. These landing ensembles are, however, also expected to be smaller in size for Cl-containing surfaces, since the ratio of rate constants for C_2H_4 combustion versus epoxidation in primary C_2H_4–O_2 surface sojourns (k_{II}/k_I) is smaller for Sample **A** versus **A**′ (0.088 versus 0.23; Table 1). Combustion occurs upon O_2^* dissociation (Step II(b); Scheme 3) and epoxidation when O_2^* is retained as molecularly bound dioxygen (Steps I(a) and I(b)), with the former prevailing with increasing landing ensemble size.

Figure 12 shows results from the same three-step CO reaction experiment (holding at 233 K and then heating to (0.33 K s^{-1}) and holding at 548 K) upon the treatment that retains O_2^* and labile O^* at interstitial landing ensembles (cooling to 233 K in flowing O_2 after thermal reductive (1.0 kPa CO) and oxidative (4.0 kPa O_2) treatments at 548 K) for

Samples **A**′ (solid) and **A** (dotted), which were collected after C_2H_4–O_2 reactions in, respectively, the absence and presence of C_2H_5Cl and previously shown to have refractory adlayers comprising solely O^* and both Cl^* and O^*, respectively (Section 2.5); the solid curves in Figure 12 are identical to those in Figure 11. CO_2 also readily forms at 233 K on samples containing refractory Cl^* adlayers (**A**). The amount of CO_2 formed at the initial sub-ambient temperature is larger when the refractory adlayer contains Cl^* and O^* compared to when it comprises solely O^* (0.0012 versus 0.00063 CO_2 per total Ag for, respectively, **A** and **A**′; Table 2), which contrasts the lower rates of C_2H_4–O_2 and N_2O reactions and O^* uptakes observed in the presence of Cl^*. The total amount of CO_2 formed throughout the entirety of the experiment is, however, smaller for the Cl^* containing sample, consistent with previous results which showed that fewer interstitial landing ensembles form when the refractory adlayer includes Cl^*. The higher absolute and relative (0.21 versus 0.089 ($=0.00063/0.0071$)) amounts of CO_2 formed at 233 K indicates that refractory Cl^* adlayers are denser and form smaller landing ensembles that retain higher fractions of highly reactive O_2^* relative to labile and recalcitrant O^* species.

The addition of O-atoms via N_2O decomposition and the removal of O_2-derived species by CO provide compelling evidence for formation of refractory adlayers consisting of O^* or O^*/Cl^* species on Ag nanoparticle surfaces during C_2H_4–O_2 reactions in the absence or presence of C_2H_5Cl moderators, respectively. Refractory O^* adlayers can be removed by thermal reductive treatments in flowing CO (1.0 kPa, 548 K), but Cl adatoms are more persistent; they are not removed by CO and
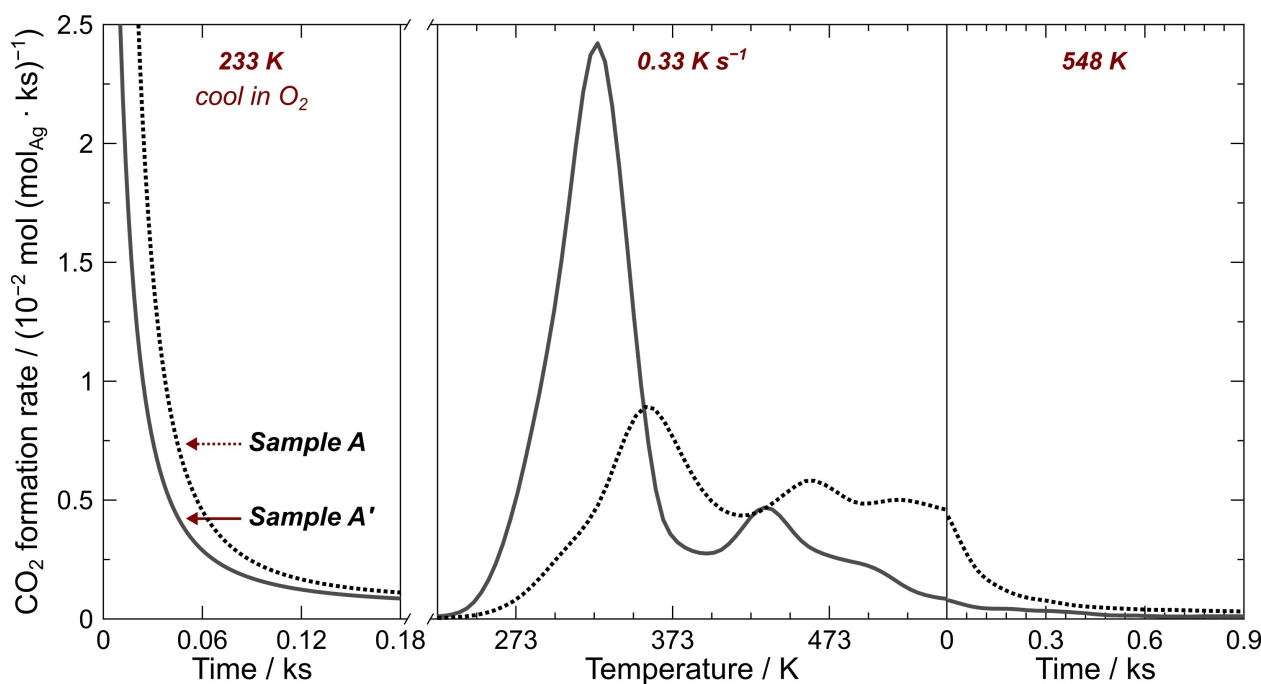

Figure 12. CO_2 formation rates upon contacting Ag/α-Al_2O_3 (18 % wt. Ag) samples (Samples **A**′ (solid) and **A** (dotted); collected after C_2H_4–O_2 reactions in the absence and presence of C_2H_5Cl, respectively; Table 3) with a CO (1.0 kPa) stream while holding at 233 K (*left*), then heating at 0.33 K s^{-1} to (*middle*), and holding at (*right*) 548 K. Prior to CO exposure, the samples were treated sequentially in reductive (1.0 kPa CO, 548 K) and oxidizing (4.0 kPa O_2) environments at 548 K and then cooled to 233 K in flowing O_2 (4.0 kPa).

ChemCatChem

Research Article
doi.org/10.1002/cctc.202301369

Chemistry
Europe
European Chemical
Societies Publishing

require $> 10^4$ O_2 conversion turnovers to be removed by CH_4 and C_2H_4 during EO synthesis reactions (Figure 3). The refractory mosaic contains interstices that serve as "landing ensembles" for kinetically-relevant O_2 activation, but inhibit O_2 dissociation (Step II(b), Scheme 3), a process that converts an electrophilic O-atom in O_2 to nucleophilic O* species. These small interstices act as isolated redox-active ensembles that destabilize the transition states that mediate dissociation steps preferentially over those involved in the scavenging of the electrophilic O-atom in O_2* (by C_2H_4 or CO). Highly reactive dioxygen species that engage in electrophilic C–H insertion and epoxidation are encountered at diiron active sites of methane monooxygenases,[74] dicopper sites grafted onto ion-exchange centers in aluminosilicates,[75] and isolated $2e^-$ redox centers within mixed Ce–Zr oxides[76] and polyoxometalates.[77,78] The O* refractory adlayer inhibits (O–O)* dissociation even in the absence of persistent Cl* species, but their presence leads to denser adlayers with fewer (and plausibly smaller) interstices, as evidenced by the lower O* uptakes and N_2O and C_2H_4–O_2 rates and the higher coverages of highly-reactive O_2* species on Ag nanoparticles exposed to C_2H_5Cl. Ag surfaces with refractory adlayers comprising Cl* lead to higher primary selectivities (or, equivalently, smaller k_{II}/k_I ratios, Table 1) compared to those with only O* because they are more effective at retaining O_2*. The presence of persistent Cl adatoms reduces the frequency of occasional and local disruptions to O adlayers that arise upon desorption by combining with the nucleophilic O* formed when consuming the electrophilic O-atom in O_2* in epoxidation events to unveil larger landing ensembles that favor dissociative adsorption.

3. Conclusions

C_2H_4–O_2 reactions were conducted on catalysts comprising Ag particles dispersed on α-Al_2O_3 supports without and with Re and Cs additives and in the absence and presence of C_2H_5Cl in reactant streams to assess the effects of these promoters (Re and Cs) and moderators (C_2H_5Cl) on rates and ethylene oxide (EO) selectivities. The observed EO:CO_2 molar ratios were always less than the 3:1 ratio prescribed by mechanistic frameworks in which only one O-atom within O_2 is delivered to C_2H_4 in an electrophilic epoxidation event to give EO and the other is scavenged in a cascade of oxidation events, initiated upon H-abstraction from C_2H_4 by a nucleophilic O-adatom, to give combustion products. These selectivity losses occur in primary C_2H_4–O_2 sojourns and via secondary EO combustion reactions, evidenced by EO/CO_2 ratios that were less than three, even as O_2 conversions asymptotically approached zero, and EO selectivities that decreased monotonically with increasing conversion. Selectivity losses in single surface sojourns can be ascribed to dissociation of O–O bonds within bound dioxygen intermediates (O_2*) that form in kinetically-relevant O_2 activation steps; this bypasses the utilization of electrophilic O-atoms in desired epoxidation events and forms excess nucleophilic O-adatoms (O*) that lead to excess C_2H_4 combustion. Measured selectivity versus conversion datasets for each catalyst were accurately captured by a model parameterized by two ratios of apparent rate constants: one for C_2H_4 combustion versus epoxidation (k_{II}/k_I) and another for EO combustion in secondary channels versus O_2 consumption in primary reactions ($k_{2\circ}/k_{1\circ}$).

The incorporation of Re into Ag/α-Al_2O_3 catalysts (18 % wt. Ag; 380:1 Ag:Re, atom ratio) led to slightly lower O_2 consumption rates (< 2-fold decrease) and similar k_{II}/k_I but larger $k_{2\circ}/k_{1\circ}$ values compared to the unpromoted catalyst. These results indicate that the Re domains that form upon the preparation and treatment protocols used herein block Ag surface site ensembles from activating O_2 but do not alter the intrinsic reactivity properties of the ensembles that determine whether O_2* participates in epoxidation or undergoes O–O bond cleavage. The increase in $k_{2\circ}/k_{1\circ}$ reflects the introduction of additional acid centers that catalyze the isomerization and hydrolysis of EO to form reactive intermediates (CH_3CHO and $(CH_2OH)_2$, respectively) that more readily undergo H-abstraction by O* than EO. The addition of Cs led to smaller $k_{2\circ}/k_{1\circ}$ values for both the Cs-promoted and Re, Cs-copromoted catalysts relative to the unpromoted Ag/α-Al_2O_3 catalyst, showing that Cs neutralizes acid centers that are native to the α-Al_2O_3 support as well as those introduced when incorporating Re. The Cs-promoted sample, similar to the Re-promoted one, showed slightly lower O_2 consumption rates, but the Re, Cs-copromoted sample did not exhibit such inhibition, suggesting the formation of Re–Cs adducts that preferentially reside on α-Al_2O_3 versus Ag surfaces. O_2 conversion rates and k_{II}/k_I values were larger, by 10- and 3-fold, respectively, and $k_{2\circ}/k_{1\circ}$ values were unchanged when C_2H_4–O_2 reactions were performed on the unpromoted Ag/α-Al_2O_3 catalyst in the absence versus in the presence of C_2H_5Cl moderators (0.80–6.3 Pa C_2H_5Cl, $> 10,000:1$ CH_4:C_2H_5Cl, and $> 10,000:1$ C_2H_4:C_2H_5Cl). These results demonstrate that alkyl chlorides deposit strongly bound Cl* adatoms that reduce the number of available Ag surface site ensembles for O_2 activation and that the resulting refractory Cl* adlayer decreases the relative rate at which O_2* undergoes O–O bond cleavage versus electrophilic addition to C_2H_4 for EO synthesis.

N_2O probe reactions showed that Ag/α-Al_2O_3 samples, both with and without the refractory Cl* adlayer, accumulate strongly bound O-adatoms until reaching a sufficiently high coverage at which inter-atom repulsive forces weaken O* binding and destabilize N_2O decomposition transition states to enable stable N_2 and O_2 evolution rates (in a 2:1 N_2:O_2 molar ratio). This result demonstrates that the Ag surface site ensembles that turn over in catalytic cycles are those formed at interstices of refractory adlayers. O-adatom uptakes, stoichiometric O* addition rates, and catalytic N_2O decomposition rates were all approximately 10-fold smaller when the Ag particles contained strongly bound Cl-adatoms, which, unlike the strongly bound O-adatoms, could not be removed by prolonged thermal treatments in reducing environments (1.0 kPa CO, 548 K). Thus, the "landing ensembles" available for O_2 activation (in EO synthesis) and evolution (in N_2O decomposition catalysis) are fewer in number when the refractory adlayer comprises both Cl* and O* instead of solely O*.

Probe reactions for O-removal by CO from O_2-treated Ag/α-Al_2O_3 samples (4.0 kPa O_2, 548 K) showed that loosely-bound

ChemCatChem

Research Article
doi.org/10.1002/cctc.202301369

Chemistry Europe
European Chemical
Societies Publishing

O_2-derived species, which readily react with CO to give CO_2 at 233 K, can form on Ag surfaces. These highly-reactive adsorbates are likely to be dioxygen species bound at interstices of refractory O^*/Cl^* adlayers, since they are formed only on Ag surfaces featuring strongly bound O- and Cl-adatoms (the deposition of which occurs at elevated temperatures) and retained with appreciable coverages only when the samples are cooled to sub-ambient temperatures in a surrounding environment that contains O_2. The relative amount of highly-reactive O_2^* versus strongly bound O^* increased on Ag samples with mixed Cl^*/O^* instead of solely O^* adlayers, which reflects the requirement of larger site ensembles for (O–O)* bond dissociation versus smaller ones for O_2^* consumption by CO (and C_2H_4) reductants. Thus, the "landing ensembles" are not only fewer in number but also smaller in size when refractory adlayers contain persistent Cl adatoms.

In EO synthesis, the occasional recombinative desorption of O^*, which involves adatoms at interstitial sites and/or at peripheries of refractory adlayers, momentarily opens larger landing ensembles that favor (O–O)* bond cleavage, leading to excess coverages of nucleophilic O-atoms and combustion of C_2H_4. These occurrences become less frequent when refractory adlayers contain Cl^*, which, in turn, leads to higher EO selectivities in primary C_2H_4–O_2 sojourns, or, equivalently, smaller k_{II}/k_I values. The isolated landing ensembles that form at interstices of refractory adlayers on Ag surfaces give rise to O_2 reactivity patterns that are like those encountered in other systems for aerobic oxidation catalysis — for example, metalloproteins and metal oxide clusters — in which O_2 activation is known to proceed via intermediates (O_2^* and O^*) with distinct reactivity (electrophilic epoxidation/C–H insertion and nucleophilic C–H cleavage).

Experimental Methods

Catalyst preparation and characterization

Ag/α-Al_2O_3 (18 % wt. Ag) was prepared by impregnating α-Al_2O_3 extrudates (> 99.5 %; 2.1 $m^2 g^{-1}$; Exacer Catalyst Support) with an aqueous (deionized water) solution of a silver ethylenediamine oxalate complex, which was prepared using established procedures;[79,80] briefly, Ag_2O powders (> 99.9 %, Ames-Goldsmith) were slowly added to a stirring aqueous solution of $C_2H_4(NH_2)_2$ (> 99 %, Alfa-Aesar) and (COOH)$_2 \cdot 2H_2O$ (> 99.6 %) held at 308 K to give a grey-yellow clear liquid. The impregnated solids were dried under vacuum (80 mbar) at ambient temperature and subsequently treated in flowing N_2 (< 8 ppmv O_2; 30 $cm^3 s^{-1} g^{-1}$) at 563 K (0.50 $K s^{-1}$) for 0.72 ks. The resulting material is denoted here as Sample **A** (Table 3).

Re and Cs were introduced into Ag/α-Al_2O_3 by impregnating aliquots of Sample **A** with an aqueous solution of NH_4ReO_4 (> 99.9 %, Buss & Buss Spezialmetalle GmbH) and $C_2H_4(NH_2)_2$, CsOH(aq) (HC Starck), and mixtures thereof followed by the same drying and thermal treatment steps used for Sample **A**. Table 3 lists the nominal elemental compositions of Samples **A**, **B** (+ Re), **C** (+ Cs), and **D** (+ Re, Cs). Elemental analyses show excellent agreement between nominal and measured compositions; for Sample **D**, the measurements correspond to: 17.9 % wt. Ag, 380:1 Ag:Re, and 390:1 Ag:Cs.

Table 3. Nominal Ag, Re, and Cs contents for Samples **A–D**.

	Composition		
	Ag (wt. fraction)	Ag:Re (atom ratio)	Ag:Cs (atom ratio)
A′	0.18	∞	∞
A	0.18	∞	∞
B	0.18	380	∞
C	0.18	∞	380
D	0.18	380	380

C_2H_4–O_2 reactions on Sample **A′** were conducted without C_2H_5Cl in reactant mixtures.

X-ray diffraction patterns (Bruker D8 Advance; Cu–Kα, 0.15406 nm) of as-prepared samples exhibited lines for α-Al_2O_3 and cubic Ag crystals. Scanning electron micrographs (SEM) were obtained using a microscope equipped with a Schottky-emission electron gun (Thermo Scientific Apreo 2) set to an acceleration voltage of 5 keV. Ag particle size distributions were measured from > 1500 particles and used to calculate surface-averaged particle diameters ($\langle d_{SEM} \rangle$):

$$\langle d_{SEM} \rangle = \frac{\sum n_i d_i^3}{\sum n_i d_i^2} \tag{20}$$

where n_i is the number of particles with a diameter d_i. Values of fractional dispersion (Đ), defined as the ratio between the numbers of surface to total Ag atoms, were estimated by assuming hemispherical crystallites with atomic density of bulk Ag:[81]

$$Đ = \frac{1.18}{(\langle d_{SEM} \rangle / nm)} \tag{21}$$

Catalytic testing

C_2H_4–O_2 reactions were conducted in a stainless steel downflow tubular reactor packed with a bed of catalyst aggregates (21.0 g, 1.0–1.6 mm) placed between layers of inert steatite balls. The reactor was heated by a recirculating oil bath, which provided uniform temperature at zones surrounding the packed bed. Samples were treated in flowing N_2 (30 $cm^3 s^{-1} g^{-1}$) at 483 K for 15 h before exposure to C_2H_4 and O_2 reactants. Reactor influent mixtures comprised CH_4, H_2O, C_2H_4, O_2, CO_2, and C_2H_5Cl at concentrations typical to those of the recycle gas in commercial EO processes (vide infra). Gas flow rates were controlled by mass flow controllers, and H_2O was introduced by passing the stream through a saturator filled with deionized water and held at 291 K and 16 bar. Inlet and outlet fluid compositions were analyzed using mass spectrometry (Thermo Fisher Prima PRO). EO, CO_2, and H_2O were the only products formed in detectable quantities, and calculated C, H, and O atom balances between inlet and outlet streams closed within ± 1.0 %.

Prior to C_2H_4–O_2 reactions, a careful sample "break-in" protocol was used to avoid thermal runaway and the concomitant chemical and structural changes that would otherwise belie the effects of promoters, temperature, residence time, and reactant and moderator pressures on rates and selectivities. The reactor was pressurized to 16 bar in flowing N_2 at 453 K, and N_2 was then sequentially replaced by CH_4, CO_2, H_2O, C_2H_4, C_2H_5Cl, and finally O_2 to give an inlet reactor mixture comprising 64 kPa O_2, 340 kPa C_2H_4, 16 kPa

ChemCatChem

Research Article
doi.org/10.1002/cctc.202301369

Chemistry Europe
European Chemical
Societies Publishing

CO_2, 1.6 kPa H_2O, and 4 Pa C_2H_5Cl, with CH_4 as the balance gas, at a total flow rate that corresponds to a residence time, per total Ag, of 0.50 ks·(mol Ag)·(mol O_2)$^{-1}$. The temperature was increased stepwise to 493 K, and the "break-in" protocol, for Samples **A**, **B**, **C**, and **D** (Table 3), was finalized after allowing C_2H_4–O_2 reaction to proceed at this condition for 72 h. The "break-in" procedure for Sample **A′** (unpromoted Ag/α-Al_2O_3 tested in the absence of C_2H_5Cl; Table 3) was similar but without C_2H_5Cl and a final reaction temperature and duration of 463 K and 168 h (instead of 493 K and 72 h).

Samples were retrieved after catalytic testing in C_2H_4–O_2 reactions by suspending reactor heating, switching the inlet stream to a N_2 purge (2.0 cm^3 s^{-1} g^{-1}), and cooling to <363 K at 16 bar before depressurizing and collecting the catalyst aggregates. These "spent" samples were examined using the described characterization methods (Section 4.1) and in probe reactions (Section 4.3) with intent of evaluating any reaction induced alterations to their structural and chemical properties.

O-atom addition and removal reactions

Aggregates (180–250 μm) of as-prepared and "spent" analogues of Samples (**A′** and **A**–**D**) were placed within a fritted quartz "U"-tube reactor (10 mm i.d.) that was held within a resistively heated furnace (National Element FA120) with temperature measured and regulated with a K-type thermocouple (Omega) and an electronic controller (Watlow 96). Samples were treated in flowing He ($>99.999\%$, Airgas; 0.67–2.7 cm^3 g^{-1} s^{-1}) at 548 K (0.083 K s^{-1}) for 12 h prior to cooling to the target temperature (233 K) and/or exposure to reactant mixtures; sub-ambient reactor temperatures were achieved by continuously flowing liquid N_2 into the insulated furnace. Flow rates of influent reactor mixtures were metered by mass flow controllers (Porter 201), which comprised O_2 (20% O_2/He; Airgas, primary standard), N_2O (3.0% N_2O/3.0% Ar/He; Praxair, certified standard), Ar (5.0% Ar/He; Praxair, primary standard) and He for O-addition reactions and CO (10% CO/He; Praxair, certified standard), Ar, and He for O-removal reactions. Reactor inlet and exit streams were analyzed using sequential infrared (MKS Multi Gas Analyzer 2030) and mass (Leybold Inficon Transpector 2.0) spectrometers. For reactions involving N_2O, a cold trap held at 77 K was placed between the two detectors to allow robust assessment of N_2 without conflating contributions from N_2O fragments in the recorded mass spectra.

Supporting Information

Additional references cited within the Supporting Information.[82,83]

Acknowledgements

Conflict of Interests

The authors declare no conflict of interest.

Data Availability Statement

The data that support the findings of this study are available from the corresponding author upon reasonable request.

[1] P. P. McClellan, *Ind. Eng. Chem.* **1950**, *42*, 2402–2407.
[2] T. E. Lefort (Francaise De Catalyse Generalisee SA), US 1998878, **1935**.
[3] J. M. Berty, *Ethylene Oxide Synthesis, In Applied Industrial Catalysis*, Vol. 1, B. L. Leach, Eds.; Academic Press, New York **1983**, pp. 207–238.
[4] J. P. Dever, K. F. George, W. C. Hoffmann, H. Soo, *Ethylene Oxide, In Kirk-Othmer Encyclopedia of Chemical Technology*, 5th ed.; John Wiley & Sons, Hoboken, NJ **2004**, pp. 632–673.
[5] S. Rebsdat, D. Mayer, *Ethylene Oxide, In Ullmann's Encyclopedia of Industrial Chemistry*, Wiley-VCH Verlag GmbH, Weinheim **2012**, pp. 547–572.
[6] J. H. Teles, I. Hermans, G. Franz, R. A. Sheldon, *Oxidation, In Ullmann's Encyclopedia of Industrial Chemistry*, Wiley-VCH Verlag GmbH, Weinheim **2015**, pp. 1–103.
[7] J. R. Lockemeyer, *The Shell Ethylene Oxide Catalyst Journey*, At *Catalysis Club of Philadelphia Annual Symposium*, May 24 **2023**.
[8] J. H. Miller, A. Joshi, X. Li, A. Bhan, *J. Catal.* **2020**, *389*, 714–720.
[9] M. Schwarzmann, W.-D. Mroß, K.-H. Böhning, *Chem. Ing. Tech.* **1988**, *60*, 657–661.
[10] J. E. van den Reijen, W. C. Versluis, S. Kanungo, M. F. d'Angelo, K. P. de Jong, P. E. de Jongh, *Catal. Today* **2019**, *338*, 31–39.
[11] J. R. Lockemeyer, T. L. Lohr, *ChemCatChem* **2023**, *15*, e202201511, https://doi.org/10.1002/cctc.202201511.
[12] C.-J. Chen, J. W. Harris, A. Bhan, *Chem. Eur. J.* **2018**, *24*, 12405–12415.
[13] T. Pu, H. Tian, M. E. Ford, S. Rangarajan, I.E. Wachs, *ACS Catal.* **2019**, *9*, 10727–10750.
[14] M. Matusz, M. A. Richard, M. L. Hess (Shell USA Inc), US 8932979, **2015**.
[15] A. Karpov, C. Walsdorff, M. Kraemer, A. Lange de Oliveira, G. Krennrich, C. Bartosch, J. Zuehlke (BASF SE), EP 3749450, **2022**.
[16] K. Smoll, J. Van Noyen, J. H. Pazmino, V. P. Santos Castro, M. H. McAdon, A. Liu (Dow Global Technologies LLC), WO 2023287500, **2023**.
[17] M. M. Bhasin, P. C. Ellgen, C. D. Hendrix (Union Carbide Chemicals and Plastics Technology LLC), US 4916243, **1990**.
[18] M. M. Bhasin, C. D. Hendrix, *Stud. Surf. Sci. Catal.* **1993**, *75*, 1431–1439.
[19] A. Karpov, M. Kraemer, M. Bosch, C. Bartosch, J. Zuehlke, C. Lizandara-Pueyo, G. Wasserschaff (BASF SE), US 11400437 B2, **2022**.
[20] A. M. Lauritzen (Shell USA Inc), US 4766105, **1988**.
[21] R. B. Grant, R. M. Lambert, *J. Catal.* **1985**, *93*, 92–99.
[22] C. T. Campbell, *J. Phys. Chem.* **1985**, *89*, 5789–5795.
[23] C. T. Campbell, K. A. Daube, *J. Catal.* **1987**, *106*, 301–306.
[24] S. N. Goncharova, E. A. Paukshtis, B. S. Bal'zhinimaev, *Appl. Catal. A: Gen.* **1995**, *126*, 67–84.
[25] D. Ren, H. Xu, J. Li, J. Li, D. Cheng, *Mol. Catal.* **2017**, *441*, 92–99.
[26] D. A. Bulushev, E. A. Paukshtis, Y. N. Nogin, B. S. Bal'zhinimaev, *Appl. Catal. A: Gen.* **1995**, *123*, 301–322.
[27] D. M. Minahan, G. B. Hoflund, W. S. Epling, D. W. Schoenfeld, *J. Catal.* **1997**, *168*, 393–399.
[28] W. S. Epling, G. B. Hoflund, D. M. Minahan, *J. Catal.* **1997**, *171*, 490–497.
[29] P. A. Kilty, W. M. H. Sachtler, *Catal. Rev. Sci. Eng.* **1974**, *10*, 1–16.
[30] M.-H. Baik, M. Newcomb, R. A. Friesner, S. J. Lippard, *Chem. Rev.* **2003**, *103*, 2385–2420.
[31] D. Jingfa, Y. Jun, Z. Shi, Y. Xiaohong, *J. Catal.* **1992**, *138*, 395–399.
[32] J. C. Dellamorte, J. Lauterbach, M. A. Barteau, *Catal. Today* **2007**, *120*, 182–185.
[33] W. Diao, C. D. DiGiulio, M. T. Schaal, S. Ma, J. R. Monnier, *J. Catal.* **2015**, *322*, 14–23.
[34] M. A. Salaev, A. A. Salaeva, O. K. Poleschuk, O. V. Vodyankina, *J. Struct. Chem.* **2019**, *60*, 1713–1724.
[35] H. Xu, L. Zhu, Y. Nan, Y. Xie, D. Cheng, *ACS Catal.* **2021**, *11*, 3371–3383.
[36] M. A. Salaev, A. A. Salaeva, O. V. Vodyankina, *Catal. Today* **2021**, *375*, 585–590.
[37] B. W. J. Chen, B. Wang, M. B. Sullivan, A. Borgna, J. Zhang, *ACS Catal.* **2022**, *12*, 2540–2551.
[38] R. B. Grant, R. M. Lambert, *J. Catal.* **1985**, *92*, 364–375.

[39] R. B. Silverman, *The Organic Chemistry of Enzyme-Catalyzed Reactions*, Academic Press **2002**, pp. 227–249.

[40] L. Que Jr., R. C. Kolanczyk, L. S. White, *J. Am. Chem. Soc.* **1987**, *109*, 5373–5380, https://doi.org/10.1021/ja00252a012.

[41] A. M. Orville, J. D. Lipscomb, D. H. Ohlendorf, *Biochemistry* **1997**, *36*, 10052–10066.

[42] R. B. Silverman, *The Organic Chemistry of Enzyme-Catalyzed Reactions*, Academic Press **2002**, pp. 175–226.

[43] J. D. Lipscomb, *Annu. Rev. Microbiol.* **1994**, *48*, 371–399.

[44] P. Besse, H. Veschambre, *Tetrahedron* **1994**, *50*, 8885–8927.

[45] M. A. Barteau, R. J. Madix, *Surf. Sci.* **1980**, *97*, 101–110.

[46] V. I. Bukhtiyarov, I. P. Prosvirin, R. I. Kvon, *Surf. Sci.* **1994**, *320*, L47–L50.

[47] L. M. Slaughter, J. P. Collman, T. A. Eberspacher, J. I. Brauman, *Inorg. Chem.* **2004**, *43*, 5198–5204.

[48] J. K. Leigh, J. Rajput, D. E. Richardson, *Inorg. Chem.* **2014**, *53*, 6715–6727.

[49] V. Vargheese, Y. Kobayashi, S. T. Oyama, *Angew. Chem. Int. Ed.* **2020**, *59*, 16644–16650.

[50] R. E. Kenson, M. Lapkin, *J. Phys. Chem.* **1970**, *74*, 1493–1502.

[51] H. R. Dettwiler, A. Baiker, W. Richarz, *Helv. Chim. Acta* **1979**, *62*, 1689–1700.

[52] S. A. Tan, R. B. Grant, R. M. Lambert, *J. Catal.* **1987**, *106*, 54–64.

[53] G. H. Twigg, *Proc. Roy. Soc. A* **1947**, *188*, 92–104, https://doi.org/10.1098/rspa.1946.0099.

[54] R. Aris, *Elementary Chemical Reactor Analysis*, Butterworth-Heinemann **1989**, pp. 259–321.

[55] K. R. Iyer, A. Bhan, *J. Catal.* **2023**, *420*, 99–109.

[56] J. C. Dellamorte, J. Lauterbach, M. A. Barteau, *Top. Catal.* **2010**, *53*, 13–18.

[57] P. H. Keijzer, J. E. van den Reijen, C. J. Keijzer, K. P. de Jong, P. E. de Jongh, *J. Catal.* **2022**, *405*, 534–544.

[58] M. Giesen, D. M. Kolb, *Surf. Sci.* **2000**, *468*, 149–164.

[59] M. Mesgar, P. Kaghazchi, T. Jacob, E. Pichardo-Pedrero, M. Giesen, H. Ibach, N. B. Luque, W. Schmickler, *ChemPhysChem* **2013**, *14*, 233–236.

[60] C. T. Campbell, *J. Catal.* **1986**, *99*, 28–38.

[61] J. W. Harris, A. Bhan, *J. Catal.* **2019**, *380*, 318–331.

[62] J. W. Harris, J. A. Herron, J. F. DeWilde, A. Bhan, *J. Catal.* **2019**, *377*, 378–388.

[63] M. Bowker, K. C. Waugh, *Surf. Sci.* **1983**, *134*, 639–664.

[64] J. R. Lockemeyer, R. C. Yeates, D. Reinalda (Shell Oil Company), US 8148555, **2012**.

[65] H. Shibata, A. G. Basrur, S. Gopal, M. H. McAdon, A. C.-Y. Liu, L. Zhang, E. R. Frank (Dow Technology Investments LLC), US 9649621, **2017**.

[66] Y.-R. Luo, *Handbook of Bond Dissociation Energies in Organic Compounds*, CRC Press **2002**.

[67] J. K. Lee, X. E. Verykios, R. Pitchai, *Appl. Catal.* **1988**, *44*, 223–237.

[68] M. Stoyanova, U. Rodemerck, U. Bentrup, U. Dingerdissen, D. Linke, R.-W. Mayer, H. G. J. Lansink Rotgerink, T. Tacke, *Appl. Catal. A: Gen.* **2008**, *340*, 242–249.

[69] H. Pines, W. O. Haag, *J. Am. Chem. Soc.* **1960**, *82*, 2471–2483.

[70] C.-F. Mao, M. A. Vannice, *Appl. Catal. A* **1995**, *122*, 61–76.

[71] A. W. Czanderna, *J. Vac. Sci. Technol.* **1977**, *14*, 408–411, https://doi.org/10.1116/1.569243.

[72] A. J. Capote, J. T. Roberts, R. J. Madix, *Surf. Sci.* **1989**, *209*, L151–L156.

[73] U. Burghaus, H. Conrad, *Surf. Sci.* **1996**, *364*, 109–121.

[74] A. M. Valentine, S. S. Stahl, S. J. Lippard, *J. Am. Chem. Soc.* **1999**, *121*, 3876–3887.

[75] M. H. Groothaert, J. A. van Bokhoven, A. A. Battiston, B. M. Weckhuysen, R. A. Schoonheydt, *J. Am. Chem. Soc.* **2003**, *125*, 7629–7640.

[76] V. V. Pushkarev, V. I. Kovalchuk, J. L. d'Itri, *J. Phys. Chem. B* **2004**, *108*, 5341–5348.

[77] I. A. Weinstock, R. E. Schreiber, R. Neumann, *Chem. Rev.* **2018**, *118*, 2680–2717.

[78] S. Kwon, P. Deshlahra, E. Iglesia, *J. Catal.* **2018**, *364*, 228–247.

[79] A. Karpov, A. Lehr, D. Rieck, H. Borchert, T. Weinland, M. Bosch, C. Walsdorff, C. Bartosch, J. Zuehlke (BASF SE), EP 3749449, **2022**.

[80] C. Kunz, C. Walsdorff, M. Viertelhaus, C. Adam, A. Karpov, J. Nuss, M. Jansen, *Z. Anorg. Allg. Chem.* **2021**, *647*, 1348–1353.

[81] M. Choi, Z. Wu, E. Iglesia, *J. Am. Chem. Soc.* **2010**, *132*, 9129–9137.

[82] R. J. Madon, M. Boudart, *Ind. Eng. Chem. Fundamen.* **1982**, *21*, 438–447.

[83] E. L. Cussler, *Diffusion: Mass Transfer in Fluid Systems*, 3rd ed., Cambridge University Press **2009**.